Phycological Research

Phycological Research 2021; **69:** 88–115 doi: 10.1111/pre.12448

Morphological and molecular characterization of multiple new *Azadinium* strains revealed a high diversity of non-toxigenic species of Amphidomataceae (Dinophyceae) including two new *Azadinium* species in Irish waters, North East Atlantic

Rafael Salas [1,2]* **Urban Tillmann** [2]* **Haifeng Gu** [3] **Stephan Wietkamp** [2] **Bernd Krock** [2] **and Dave Clarke** [1]

[1]Marine Institute, Galway, Republic of Ireland, [2]Alfred-Wegener-Institut, Helmholtz-Zentrum für Polar- und Meeresforschung (AWI), Bremerhaven, Germany and [3]Third Institute of Oceanography, Ministry of Natural Resources, Xiamen, People's Republic of China

SUMMARY

Shellfish contamination with azaspiracids (AZA), which are lipophilic marine biotoxins produced by marine dinoflagellates, is a major and recurrent problem for the Irish shellfish industry. AZA are produced by certain species of Amphidomataceae, but the species diversity of this group of microalgae in Irish waters is poorly known. Here we present a morphological and molecular characterization of multiple new strains of non-toxigenic *Azadinium* isolated on an oceanographic survey in 2018. A lack of AZA production for all strains presented here was demonstrated by LC-MS/MS analysis. One strain of *Azadinium caudatum* var. *margalefii* (first strain for the area) confirmed non-toxigenicity of Atlantic populations of this species. One strain designated as *Azadinium* cf. *zhuanum* was similar to *Az. zhuanum* described from China but differed from the type strain in nucleus position, by the dominant number of apical plates, and by significant differences in rRNA gene sequences. Finally, two new non-toxigenic *Azadinium* species are described from the North East Atlantic: *Azadinium galwayense* sp. nov. and *Azadinium perfusorium* sp. nov. *Azadinium galwayense* differed from other *Azadinium* by a characteristic combination regarding presence and location of the ventral pore (vp; on the right side of the pore plate), of a pyrenoid (located in the episome), and by a pentagonal shape of the median anterior intercalary plate 2a, and lack of contact between plates 1″ and 1a. *Azadinium perfusorium* shared the same vp position as *Az. galwayense* and differed by a characteristic combination of a pyrenoid located in the hyposome, a tetragonal shape of plate 2a, and a relatively large size of the two lateral anterior intercalary plates. Molecular phylogeny confirmed the distinctiveness of these two new species and their placement in *Azadinium*. The present findings significantly increased knowledge on the diversity of *Azadinium* species in the North East Atlantic.

Key words: azaspiracids, biogeography, new species, phylogeny.

INTRODUCTION

The Amphidomataceae is an increasingly growing family of Dinophyceae since the initial discovery of *Azadinium spinosum* Elbrächter & Tillmann (Tillmann *et al*. 2009) as the putative causative organism of azaspiracid (AZA) toxins (Krock *et al*. 2009). These small nano-planktonic dinoflagellates are difficult to identify under light microscopy (LM) and likely to have been mis-identified in the past for other small gymnodinioid species or small armoured species, e.g. of *Heterocapsa* (Tillmann *et al*. 2011; Salas *et al*. 2014). Thus far, the genus *Azadinium* comprises 14 species (Tillmann *et al*. 2020), and most have been described in the last decade alone (Tillmann *et al*. 2009, 2010, 2011, 2012b, 2014a, 2020; Luo *et al*. 2013, 2017; Percopo *et al*. 2013; Tillmann & Akselman 2016; Tillmann 2018).

Amphidomatacean toxins were first detected in contaminated shellfish (blue mussels - *Mytilus edulis*) in 1995, from a batch of mussels harvested in Killary Harbour in the west coast of Ireland (McMahon & Silke 1996) following an outbreak of human illness in the Netherlands after consumption of contaminated mussels from this area. The toxin was provisionally named KT (Killary Toxin) after the origin location of the mussels, but after its isolation and chemical characterization from shellfish (Satake *et al*. 1998; Ofuji *et al*. 1999) the name was changed to "azaspiracids" which better describes this lipophilic polyether molecule composed of a secondary amine (denoted by the prefix "aza- " in IUPAC nomenclature), three spiro assemblies and a carboxylic acid.

*To whom correspondence should be addressed.
Email: *urban.tillmann@awi.de*
Email: *rafael.salas@marine.ie*

Communicating Editor: Mitsunori Iwataki.
Received 15 July 2020; accepted 18 November 2020.
[Correction added on 06 March 2021, after first online publication: Affiliation 2 was added to the author, Rafael Salas.]

The development of routine chemical analysis for the main AZA detected in shellfish (AZA-1, -2, -3) as a monitoring tool in the early 2000s have shown that concentrations above the EU regulatory level of 160 micrograms of azaspiracid equivalents per kilogram (Anonymous 2004) are often found in Irish shellfish, mainly in mussels, and occasionally in oysters (*Crassostrea gigas*), cockles (*Cerastoderma edule*) and clams (*Spisula solida*) which is a serious problem for the Irish aquaculture industry (Salas *et al*. 2011; Clarke 2020).

The taxonomic diversity and wide geographical range of Amphidomataceae is also matched by a large chemical diversity (Tillmann *et al*. 2016), and the list of AZA produced by these species has increased continuously and now comprises 26 AZA variants (Krock *et al*. 2019). AZA toxins have a worldwide distribution (Braña Magdalena *et al*. 2003; Taleb *et al*. 2006; Amzil *et al*. 2008; Torgersen *et al*. 2008; Vale *et al*. 2008; Ueoka *et al*. 2009; Álvarez *et al*. 2010; López-Rivera *et al*. 2010; Yao *et al*. 2010; Krock *et al*. 2013; Trainer *et al*. 2013; Turner & Goya 2015), but Ireland to this day remains the most affected country globally by these toxins. However, little is known about the species diversity of Amphidomataceae in Irish waters. The relatively large and easy to determine taxon recorded as *Amphidoma caudata* Halldal, which in fact is a species of *Azadinium* (Nézan *et al*. 2012), is known to occur in Irish coastal waters for a long time (Dodge 1981; O'Boyle & Raine 2007). A local strain of *Az. spinosum* was isolated from Bantry Bay, southern Ireland (Salas *et al*. 2011). Based on the prevailing toxin profile in shellfish with dominance of AZA congeners typical for *Az. spinosum* (i.e. AZA-1 and -2) (James *et al*. 2002) and based on the continuous record of *Az. spinosum* presence in the Irish monitoring program using specific PCR assays (Tillmann *et al*. 2014c; Clarke *et al*. 2020) this species is assumed to be the dominant source of AZA in Ireland (Salas *et al*. 2011; Wietkamp *et al*. 2020). However, at times there does appear to be a mismatch between AZA in shellfish and LM monitoring reports of "*Azadinium* sp." in Ireland (Tillmann *et al*. 2014c), therefore the presence of additional AZA source organisms in Irish waters cannot be ruled out. Another toxigenic species present in Ireland is *Amphidoma languida* Tillmann, Salas & Elbrächter, which was originally described based on a strain obtained from Bantry Bay, Southern Ireland (Tillmann *et al*. 2012a) and which is widely distributed around Ireland (Wietkamp *et al*. 2019b, 2020). Current morphology-confirmed diversity estimates of Irish Amphidomataceae thus include three species only (*Az. spinosum*, *Az. caudatum* (both varieties) and *Am. languida*), which is low compared to a recent amphidomatacean diversity estimate from Norwegian coastal waters where the presence of seven species was documented (Tillmann *et al*. 2018a).

Detailed knowledge on the local species inventory is important to identify other yet unknown sources of AZA and/or to evaluate the potential of local non-toxigenic species/strains for false positive signals either in LM based and/or PCR methods used in the Irish monitoring program. Therefore, in summer 2018, a research survey in the North Sea, the Celtic Sea and Irish coastal waters was undertaken. The specific focus of this survey was to increase knowledge about the diversity and distribution of Amphidomataceae and their respective toxins in Irish coastal waters and in the North Sea. Field data of this survey including qPCR-based abundance and distribution of toxigenic amphidomatacean species and their toxins are presented elsewhere (Wietkamp *et al*. 2020). In addition to these field samples, diversity of Amphidomataceae in the area was studied by on-board cell isolation and establishment of a large number of clonal amphidomatacean strains. In the present paper, the focus is a morphological, toxinological, and phylogenetic description of various non-toxigenic species/strains obtained during this survey, including the formal description of two new species of the genus *Azadinium*, supplemented by a detailed description of a strain identified as *Az*. cf. *zhuanum* and brief presentation of the first Irish strain of *Az. caudatum* var. *margalefii* (Halldal) Nézan & Chomérat.

MATERIALS AND METHODS

Sample collection and isolation of strains

Plankton samples were collected during the oceanographic survey AZAHAB (Fig. 1) (RV Heincke) between 17 July and 15 August 2018 (for a full set of stations see Wietkamp *et al*. 2020). For live cell documentation and isolation, Niskin bottle samples from three depths of the upper 30 m water column were mixed, pre-screened with 20 μm gauze and gently concentrated onto 3 μm pore size polycarbonate filter (TSTP, Millipore, Darmstadt, Germany) under gentle vacuum. *Azadinium/Amphidoma* cells were photographed using a video camera (Gryphax, Jenoptik, Jena, Germany) attached to an inverted microscope (Axiovert 200M, Zeiss, Oberkochen, Germany). Cell isolation was carried out using inverted microscopes (IX-51, Olympus, Southend-on-Sea, UK; or Axiovert 200M, Zeiss). Single cells were isolated by micropipetting and placed individually in single wells of 96 well plates (Corning, New York, NY, US) prefilled with 200 μL of filtered sea water from the sampling site. Preliminary strains were kept in a temperature-controlled incubator (Model MIR 252, Sanyo Electric Biomedical Co., Osaka, Japan) at 15 °C and 16:8 h light:dark photocycle at a photon flux density of approximately 50 μmol m^{-2} s^{-1}. Primary isolation plates from the cruise were inspected in the laboratory using a stereomicroscope (SZHILLD, Olympus) for the presence of *Azadinium*-like cells as inferred from the typical size, shape, and swimming behaviour. From each positively identified well, a clonal strain was established by isolation of single cells with a micro-capillary. Established cultures were thus clonal but not axenic, and were routinely held in 65 mL plastic culture flasks at 15 °C and a photon flux density of 50 μmol m^{-2} s^{-1} on a 16:8 h light:dark photocycle. The medium was natural, sterile-filtered (0.2 μm VacuCap filters, Pall GmbH, Dreieich, Germany) Antarctic seawater (salinity: 34, pH adjusted to 8.0) and enriched with 1/10 strength K-medium (Keller *et al*. 1987), slightly modified by omitting the addition of ammonium ions.

Morphological characterization of strains

Light microscopy (LM) observations of live or preserved material of the different Amphidomataceae strains collected at mid- or late exponential growth phase were carried out using differential interference contrast (DIC) or epifluorescence and

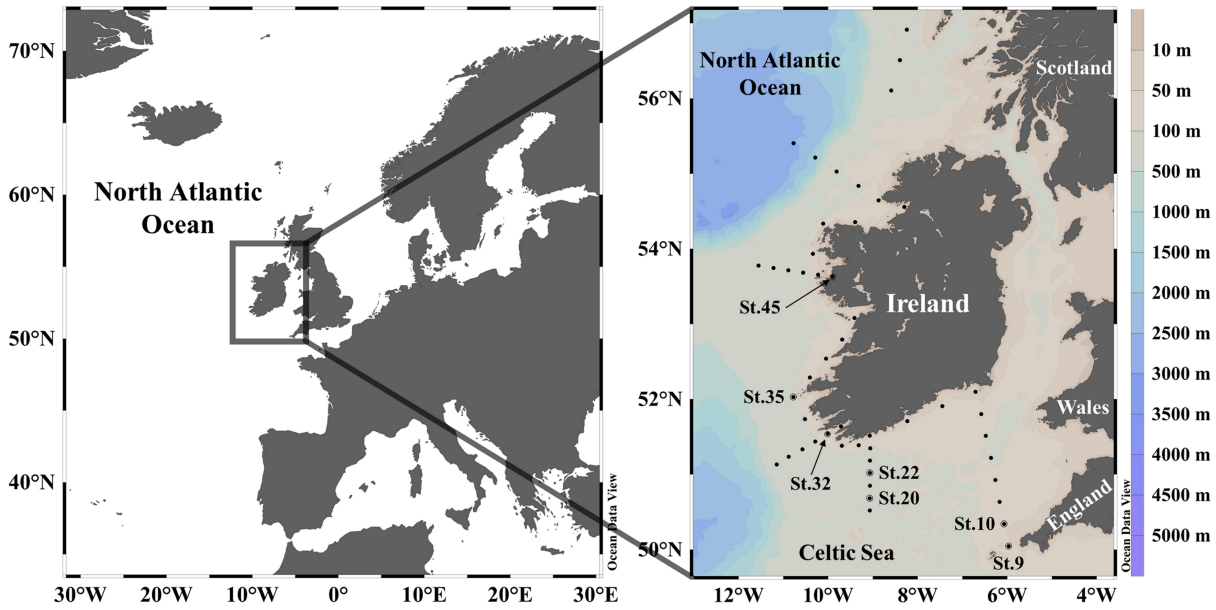

Fig 1. Map of Ireland showing sample stations where *Azadinium* strains were isolated. [Color figure can be viewed at wileyonlinelibrary.com]

high resolution (up to 1000× magnification) Axiovert 200M and Axioskop 2 (both Zeiss; both coupled with a digital camera (MRC5, Zeiss) and a video camera (Gryphax, Jenoptik, Jena, Germany), or BX-53 (Olympus) coupled with a digital camera DP72 (Olympus). Cell length and width of >50 randomly chosen cells were measured at 1000× magnification in the Axioskop 2 and the Olympus BX-53 microscopes using Axiovision software (Zeiss) or Cell Sens software dimensions (Olympus) in newly fixed cells (formaldehyde, final concentration 1%). For scanning electron microscopy (SEM) cells were collected by centrifugation (5810 R, Eppendorf, Hamburg, Germany; 3220 *g*, 10 min.) of 15 mL of culture collected at mid- or late exponential growth phase. The supernatant was removed and the cell pellet resuspended in 60% ethanol in a 2 mL microtube for 1 h at 4 °C to strip off the outer cell membrane. Subsequently, cells were pelleted by centrifugation (5415R, Eppendorf, 16 000 *g*, 5 min), fixed with formaldehyde (2% final concentration in a 60:40 mixture of deionised water and seawater), and stored at 4 °C for 3 h. Finally, cells were collected on polycarbonate filters (25 mm ø, 3 μm pore-size, Merck Millipore, Billerica, USA) in a filter funnel where all subsequent washing and dehydration steps were carried out. Eight washings (2 mL deionized water each) were followed by a dehydration series in ethanol (30, 50, 70, 80, 95, 100%; 10 min each). Filters were finally dehydrated with hexamethyldisilazane (HMDS), initially 1:1 HMDS:EtOH followed by 2 × 100% HMDS, and stored under gentle vacuum in a desiccator. Filters were mounted on stubs, sputter coated (Emscope SC500, Ashford, UK; and Quorum SC7620, Quorum Tech, Sussex, UK) with gold–palladium and viewed under a scanning electron microscope (FEI Quanta FEG 200, Eindhoven, the Netherlands or a Hitachi FlexSEM 1000, Hitachi, Maidenhead, UK). SEM micrographs were presented on a black background using Adobe Photoshop 6.0 (Adobe Systems, San Jose, CA, USA) or GIMP2.10.14 (Spencer Kimball, Peter Mattis and GIMP dev. team).

AZA analysis of strains

For AZA analysis, cultures were grown at 15 °C, a photon flux density of 50 μmol m^{-2} s^{-1} with a 16:8 h light/dark photoperiod and were harvested at late exponential phase. For each harvest, cell density was determined by settling Lugol's fixed samples and counting >400 cells under an inverted microscope in order to calculate toxin cell quota. Densely grown strains (ranging from approximately 1–7 × 10^4 cells mL^{-1}) were harvested by centrifugation (5810 R, Eppendorf) at 3220 *g* for 10 min of 50 mL subsamples. The cell pellet was resuspended, transferred to a microtube, centrifuged again (Eppendorf 5415, 16 000 *g*, 5 min), and stored frozen (−20 °C) until use. For a number of selected strains, growth and harvest procedures were repeated several times to yield a high biomass for an increased sensitivity of the toxin detection method. Total number of cells harvested for these strains is listed in Table S1 in the Supporting Information.

Cell pellets were extracted with 500 μL acetone and were vortexed every 10 min during 1 h at room temperature. Homogenates were centrifuged (Eppendorf 5810 R) at 15 °C and 3220 *g* for 15 min. Supernatants were then adjusted with acetone to a final volume of 0.5 mL. The extracts were transferred to a 0.45 μm pore-size spin-filter (Millipore Ultrafree, Millipore, Burlington, USA) and centrifuged (Eppendorf 5415 R) at 800 *g* for 30 s, with the resulting filtrate transferred into a liquid chromatography (LC) autosampler vial for LC–MS/MS analysis.

Extracts of strains were screened for known AZA in the selected reaction monitoring (SRM) mode with an analytical system consisting of triple quadrupole mass spectrometer (API 4000 QTrap, Sciex, Darmstadt, Germany) equipped with a TurboSpray interface coupled to LC equipment (model LC 1100, Agilent, Waldbronn, Germany) that included a solvent reservoir, inline degasser (G1379A), binary pump (G1311A), refrigerated autosampler (G1329A/G1330B), and

temperature-controlled column oven (G1316A). Separation of AZA (5-μL sample injection volume) was performed by reverse-phase chromatography on a C8 phase. The analytical column (50 × 2 mm) was packed with 3 μm Hypersil BDS 120 Å (Phenomenex, Aschaffenburg, Germany) and maintained at 20 °C. The flow rate was 0.2 mL min^{-1}, and gradient elution was performed with two eluents, where eluent A was water and eluent B was acetonitrile/water (95:5 v/v), both containing 2.0 mM ammonium formate and 50 mM formic acid. Initial conditions were 8-min column equilibration with 30% B, followed by a linear gradient to 100% B in 8 min and isocratic elution until 18 min with 100% B then returning to initial conditions until 21 min (total run time: 29 min). AZA profiles were determined in the SRM mode in one period (0–18) min with curtain gas: 10 psi, CAD: medium, ion spray voltage: 5500 V, temperature: ambient, nebuliser gas: 10 psi, auxiliary gas: off, interface heater: on, declustering potential: 100 V, entrance potential: 10 V, exit potential: 30 V. SRM experiments were carried out in positive ion mode by selecting the transitions shown in Table S2 in the Supporting Information.

In addition, precursor ion experiments were performed. Precursors of the characteristic AZA fragments *m/z* 348, *m/z* 350, *m/z* 360, *m/z* 362 and *m/z* 378 were scanned in the positive-ion mode from *m/z* 500 to 1000 under the following conditions: curtain gas, 10 psi; CAD, medium; ion spray voltage, 5500 V; temperature, ambient; nebuliser gas, 10 psi; auxiliary gas, off; interface heater, on; declustering potential, 100 V; entrance potential, 10 V; collision energy, 70 V; exit potential, 12 V.

Molecular phylogeny

DNA extraction

For one part of DNA extraction, conducted at the Alfred-Wegener-Institute (Helmholtz Center for Polar- and Marine Research, Bremerhaven, Germany), a number of selected strains (Table 1) was grown in 70 mL plastic culture flasks at 15 °C under a photon flux density of 70 μmol m^{-2} s^{-1} on a 16:8 h light:dark photocycle. A total of 10 to 50 mL of healthy and growing culture (based on stereomicroscopic inspection of the live culture) were harvested by centrifugation (Eppendorf 5810R; 3220 *g*, 10 min). The supernatant was discarded and the remaining cell pellet was subsequently re-suspended and transferred to a 1.5 mL microtube together with 500 μL of the SL1 lysis buffer, both provided by the DNA extraction kit. The DNA extraction followed the manufacturer's instructions of the NucleoSpin Soil DNA extraction kit (Macherey & Nagel, Düren, Germany), with a slight variation. The bead tubes were shaken, rather than vortexed, for 45 s and another 30 s at a speed of 4.0 m s^{-1} in a cell disrupter (FastPrep FP120, Thermo-Savant, Illkirch, France).

For the second part of DNA extraction, conducted at Marine Institute (Galway, Ireland), 5–30 mL aliquots were collected in 50 mL centrifuge tubes from strains (Table 1) which were in exponential growth, and centrifuged (5804, Eppendorf) for 15 min at 3230 *g*. The majority of the supernatant was removed, leaving the cell pellet in approximately 1 mL of volume. The cell pellet was re-suspended by vortexing and transferred to a 1.5 mL microtube which was centrifuged (Minispin, Eppendorf) for 5 min at 12 200 *g*, and the supernatant discarded. DNA was extracted using the Qiagen Plant Mini DNeasy extraction kit (Qiagen, Manchester, England) in accordance with the manufacturer's protocols with minor modifications. Cellular disruption was achieved by adding glass beads (two different diameter sizes of 0.75–1.0 mm ø and 0.25–0.5 mm ø) with 400 μL of API lysis buffer (supplied with extraction kit) and placed in a bead mill mixer (MM400, Retsch, Haan, Germany) for 2 min at a frequency of 25 s^{-1}. The microtubes were transferred to a thermomixer (Comfort, Eppendorf) for an incubation period of 15 min at 65 °C with shaking, and the supernatant transferred to a QIAcube (Qiagen) for automated DNA extraction.

For both parts, 2 × 50 μL of the provided elution buffer was used (to a final elution volume of 100 μL) to maximize the overall DNA yield. The DNA of all extracts was stored at −20 °C until further processing.

DNA Sequencing

Sanger-Sequencing of strain DNA was performed for the 18S/small subunit (SSU), the Internal Transcribed Spacer region (ITS1, 5.8S rRNA gene, ITS2) and the D1/D2 region of 28S/large subunit (LSU) using the following primer sets: 1F (5′ - AAC CTG GTT GAT CCT GCC AGT - 3′) and 1528R (5′ - TGA TCC TTC TGC AGG TTC ACC TAC - 3′) for SSU (Medlin *et al*. 1988); ITSa (5′ - CCA AGC TTC TAG ATC GTA ACA AGG (ACT)TC CGT AGG T - 3′) and ITSb (5′ - CCT GCA GTC GAC A(GT)A TGC TTA A(AG)T TCA GC(AG) GG - 3′) (Adachi *et al*. 1996), or ITS1 (5′ - TCC GTA GGT GAA CCT GCG G – 3′) and ITS4 (5′ - TCC TCC GCT TAT TGA TAT GC - 3′) for ITS (White *et al*. 1990); DirF (5′ -ACC CGC TGA ATT TAA GCA TA-3′) and D2C (5′ - CCT TGG TCC GTG TTT CAA GA - 3′) for LSU (Scholin *et al*. 1994).

One part of the final sequences was gained by sending extracted DNA to Eurofins sequencing facilities (Eurofins Genomics, Ebersberg, Germany), where sequences were generated on an ABI 3730 XL sequencer (Applied Biosystems by Thermo Fisher Scientific, Waltham, Massachusetts, USA) according to internal sequencing procedures.

The second part of the sequences was generated at Marine Institute. For PCR, the GoTaq Hot Start Polymerase (Promega, Wisconsin, USA) kit was used, where the PCR reaction mixture contained 11.42 μL of water (molecular biology grade), 0.08 μL of dNTPs (25 μM), 0.2 μL of 0.1 μM Forward and Reverse primers, 4 μL of GoTaq buffer (5×), 0.1 μL of Taq Polymerase, 2 μL of $MgCl_2$ (2.5 mM) and 2 μL of DNA template to a final reaction volume of 20 μL. PCR products were generated using a PCRmax Cycler (AC 296, Thermofisher Scientific) with the following conditions for each of the regions. For ITS; 95°C at 2 min; 10 cycles of: 95°C at 50 s, 58°C at 40 s, 72°C at 1 min; 30 cycles of 95°C at 45 s, 50°C at 45 s, 72°C at 1 min and a final step of 72°C at 5 min. For LSU cycling parameters; 95°C at 2 min; 30 cycles of: 95°C at 30s, 55°C at 30s, 72°C at 2 min and a final step of 72°C at 10 min. For the SSU region, the cycling parameters were; 95°C at 5 min; 30 cycles of: 95°C at 2 min, 55°C at 2 min, 72°C at 3 min and a final step of 72°C at 10 min. The generated PCR products were checked on a 2% agarose gel (in TBE buffer, 80 mV, 30 min) to check if amplification was successful and the DNA integrity. Aliquots of the generated PCR

Table 1. Compilation of information about *Azadinium* strains obtained in this study

Species	Strain	Origin Station	Length (μm) Mean ± SD Min-max	Width (μm) Mean ± SD Min-max	l/w ratio Mean ± SD	N	Morphological analysis	Sequence data
Az. perfusorium	5-B8	35	**14.2** ± 0.7 12.9–15.7	**10.7** ± 0.7 9.3–12.0	**1.33** ± 0.05	53	LM SEM	SSU, LSU, ITS
Az. perfusorium	2-D1	35	**14.9** ± 1.0 13.2–18.0	**11.3** ± 0.9 9.0–13.1	**1.32** ± 0.06	52	LM SEM	SSU, LSU, ITS
Az. perfusorium	6-B4	45	**14.4** ± 1.0 12.2–16.8	**10.5** ± 0.9 8.9–12.7	**1.37** ± 0.06	75	LM SEM	SSU, LSU, ITS
Az. perfusorium	6-C8	22	**14.5** ± 1.0 11.8–16.5	**10.9** ± 1.0 8.9–13.2	**1.33** ± 0.06	60	LM SEM	- LSU, ITS
Az. perfusorium	9-R1	9	**14.8** ± 1.1 13.0–17.5	**11.3** ± 1.3 9.1–13.5	**1.32** ± 0.08	57	LM SEM	- LSU, ITS
Az. perfusorium	35-R3	35	-	-	-	-	LM	- LSU, ITS
Az. perfusorium	9-R2	9	**13.7** ± 1.1 11.5–15.9	**10.3** ± 1.1 8.3–12.4	**1.33** ± 0.07	52	LM SEM	- LSU -
Az. perfusorium	10-R1	10	**13.9** ± 0.9 12.3–16.3	**10.3** ± 0.8 8.8–11.9	**1.36** ± 0.07	51	LM SEM	- LSU -
Az. perfusorium	10-R2	10	**13.4** ± 1.0 11.5–15.8	**10.0** ± 0.9 8.6–12.9	**1.35** ± 0.07	55	LM SEM	- LSU -
Az. perfusorium	10-R3	10	**13.5** ± 0.8 12.2–15.5	**10.0** ± 0.9 9.1–12.1	**1.31** ± 0.07	50	LM SEM	- LSU -
Az. perfusorium	35-R2	35	-	-	-	-	LM	- LSU -
Az. perfusorium	6-A8	22	**14.2** ± 0.9 11.9–16.1	**10.2** ± 0.7 8.9–11.9	**1.39** ± 0.07	50	LM SEM	- - -
Az. perfusorium	6-B7	35	**13.8** ± 0.8 12.2–15.2	**10.3** ± 0.8 9.0–12.4	**1.34** ± 0.07	50	LM SEM	- - -
Az. perfusorium	6-D2	35	**14.6** ± 1.0 12.2–16.4	**10.8** ± 1.0 9.2–12.3	**1.36** ± 0.07	50	LM SEM	- - -
Az. perfusorium	4-F9	22	**14.4** ± 0.9 11.4–15.9	**10.9** ± 0.8 9.2–12.4	**1.32** ± 0.05	50	LM SEM	- - -
Az. perfusorium	4-H7	35	**15.0** ± 0.8 13.5–16.6	**11.2** ± 0.7 9.8–12.1	**1.34** ± 0.06	50	LM SEM	- - -
Az. perfusorium	3-F6	35	**14.9** ± 0.9 12.8–16.8	**11.2** ± 0.8 9.7–12.7	**1.33** ± 0.06	52	LM SEM	- - -
Az. perfusorium	2-C7	22	**14.7** ± 0.9 13.1–16.6	**10.6** ± 0.7 9.3–12.4	**1.39** ± 0.07	50	LM SEM	- - -
Az. perfusorium	6-G12	22	**14.6** ± 1.0 12.2–16.4	**10.8** ± 0.7 9.2–12.3	**1.36** ± 0.07	50	LM	- - -
Az. perfusorium	5-B4	35	**14.8** ± 1.0 12.5–17.1	**11.2** ± 1.0 9.2–13.3	**1.33** ± 0.06	52	LM	- - -
Az. perfusorium	2-A1	35	-	-	-	-	LM	- - -
Az. perfusorium	5-B10	22	-	-	-	-	LM	- - -
Az. perfusorium	6-C3	22	-	-	-	-	LM	- - -
Az. perfusorium	6-C11	35	-	-	-	-	LM	- - -
Az. perfusorium	6-D8	35	-	-	-	-	LM	- - -
Az. perfusorium	6-G3	22	-	-	-	-	LM	- - -
Az. galwayense	35-R4	35	**13.7** ± 1.1 11.9–15.8	**9.8** ± 0.8 8.3–12.5	**1.40 ±** 0.08	51	LM, SEM	SSU, LSU, ITS
Az. galwayense	35-R6	35	**14.3** ± 1.3 11.4–16.7	**10.8** ± 1.1 8.6–14.1	**1.33 ±** 0.06	50	LM, SEM	SSU, LSU, ITS
Az. galwayense	35-R7	35	**14.1** ± 1.3 11.5–18.4	**10.6** ± 1.3 8.5–15.1	**1.34 ±** 0.10	47	LM, SEM	SSU, LSU, ITS
Az. cf. *zhuanum*	32-R1	32	**17.2** ± 1.2 14.9–20.1	**14.2** ± 1.3 12.3–17.5	**1.21** ± 0.07	49	LM, SEM	- LSU, ITS
Az. caudatum var. *margalefii*	9-E13	20	**28.5** ± 2.4 23.7–32.0	**22.8** ± 2.3 18.2–26.6	**1.25** ± 0.06	52	LM, SEM	SSU, LSU, ITS

products were forwarded on for sequencing to SequiServe (Vatterstetten, Germany).

The third part of sequences was generated at the Alfred-Wegener-Institute. Each PCR reaction contained 16.3 μL of ultra-pure H_2O, 2.0 μL of HotMaster Taq buffer (5Prime, Hamburg, Germany), 0.2 μL of dNTPs (10 μM), 0.2 μL of each primer (10 μM), 0.1 μL of Taq Polymerase (Quantabio, Beverly, Massachusetts, USA) and 1.0 μL of extracted DNA template (10 ng μL^{-1}) to a final reaction volume of 20 μL. PCR were conducted in a Nexus Gradient Mastercycler (Eppendorf) with conditions described in Tillmann *et al.* (2020). The PCR amplicons were checked on a 1%

agarose gel (in TE buffer, 70 mV, 30 min) to verify the expected length. The PCR amplicon was purified using the NucleoSpin Gel and PCR clean-up kit (Macherey-Nagel) and sequenced directly in both directions on an ABI PRISM 3730XL (Applied Biosystems by Thermo Fisher Scientific) as described in Tillmann *et al*. (2017b). Raw sequence data were processed using the CLC Genomics Workbench 12 (Qiagen, Hilden, Germany).

Phylogenetic analysis

Newly obtained SSU, ITS-5.8S and/or partial LSU rRNA gene sequences were incorporated into available *Amphidoma*, *Azadinium* and a few outgroup sequences in GenBank (https://www.ncbi.nlm.nih.gov/genbank/). GenBank accession numbers are listed in Table S3 in the Supporting Information. Concatenated SSU, ITS-5.8S and/or partial LSU rRNA gene sequences were aligned using MAFFT v7.110 (Katoh & Standley 2013) online program (http://mafft.cbrc.jp/alignment/server/). Alignments were manually checked with BioEdit v. 7.0.5 (Hall 1999). The final alignment consisted of 3439 base pairs including introduced gaps. Completed alignments of ITS-5.8S rRNA gene sequences were imported into PAUP *4b10 software (Swofford 2002) to estimate divergence rates using simple uncorrected pairwise (p) distance matrices. The secondary structures of ITS2 sequences of *Azadinium zhuanum* Z.Luo, Tillmann & H.Gu strain TIO205 and *Az.* cf. *zhuanum* strain 32-R1 were predicted using the Mfold program (Zuker 2003). (http://mfold.rit.albany.edu/?q=mfold/RNA-Folding-Form).

For Bayesian inference (BI), the program jModelTest (Posada 2008) was used to select the most appropriate model of molecular evolution with Akaike Information Criterion (AIC). Bayesian reconstruction of the data matrix was performed using MrBayes 3.2 (Ronquist & Huelsenbeck 2003) with the best-fitting substitution model (GTR + G). Four Markov chain Monte Carlo (MCMC) chains ran for 10 000 000 generations, sampling every 1000 generations. The convergence of the MCMC chains was examined in TRACER 1.7 (Rambaut *et al*. 2018), and the first 10% of the samples were discarded as 'burn-in', well after stationarity had been reached. A majority rule consensus tree was created in order to examine the posterior probabilities (BPP) of each clade. Maximum likelihood (ML) analyses were conducted with RaxML v7.2.6 (Stamatakis 2006) on the T-REX web server (Boc *et al*. 2012). Data were analyzed using the GTR + CAT approximation and the rapid hill-climbing algorithm was used. Bootstrap support (BS) was assessed with 1000 replicates.

qPCR assay specificity

DNA of strains 2-D1, 5-B8, 6-B4 (*Az. perfusorium*), strain 9-E13 (*Az. caudatum* var. *margalefii*), strain 32-R1 (*Az.* cf. *zhuanum*) and strains 35-R4, 35-R6 and 35-R7 (*Az. galwayense*) was applied to the current species-specific qPCR assays for *Az. spinosum*, *Azadinium poporum* Tillmann & Elbrächter (Toebe *et al*. 2013) and *Am. languida* (Wietkamp *et al*. 2019b), as well as to the general Amphidomataceae assay (Smith *et al*. 2016) to check whether the assays might reveal false-positive/false negative signals for the new species/strains. The DNA was normalized to a concentration of 1 ng μL^{-1} and tested in three technical replicates each for amplification in the four qPCR assays according to the procedures described in Wietkamp *et al*. (2020). Positive controls contained 1 ng μL^{-1} of DNA of each target species (*Az. spinosum*: strain 3D9; *Az. poporum*: strain UTHD4; *Am. languida*: strain Z-LF-9-C9). The limit of quantification (LOQ) and the limit of detection (LOD) for these qPCR analyses were defined as described in Wietkamp *et al*. (2020). For the standard curves of all three species-specific qPCR assays, the resolution of dilutions applied did not allow differentiation between LOD and LOQ, which were both 0.1 pg μL^{-1}.

RESULTS

Onboard high resolution LM of live samples revealed a high diversity of Amphidomataceae in Irish waters (Fig. 2). While LM observation do not allow certain species level identification for many of the species in Figure 2, isolation and SEM characterization of clonal strains was used to better describe the species diversity. Onboard single cell isolation yielded approximately 100 new clonal amphidomatacean strains. New strains of toxigenic species (*Az. spinosum* and *Am. languida*) will be presented in detail elsewhere (Tillmann *et al*. in prep). Here, we report on the identity of 31 non-toxigenic strains which were identified based on morphology as examined by LM and SEM (selected strains) and conformed for a number of strains by rDNA sequence comparison (Table 1). One strain of *Azadinium caudatum* var. *margalefii* was isolated from stat. 20 (Table 1, Fig. 1). One strain isolated from stat. 32 (Table 1, Fig. 1) was designated as *Azadinium* cf. *zhuanum*. Three strains, all originating from stat. 35, were identified as a new species described here as *Azadinium galwayense* sp. nov. The majority of strains (26 strains) isolated from stat. 9, 10, 20, 22, 35 and 45 (Table 1, Fig. 1) were found to represent another new species, *Azadinium perfusorium* sp. nov.

Description of new species

Azadinium galwayense Salas & Tillmann sp. nov.
Figures 3–6, Figure S1 in the Supporting information

Description. Small photosynthetic thecate Dinophyceae; cells 11.4 to 18.4 μm long and 8.3 to 15.1 μm wide; cingulum broad and postmedian; epitheca conical and ending in a small but distinctly pointed apical pore; hypotheca hemispherical with a very broad and long sulcus and with a single conspicuous antapical spine slightly angled to the right; tabulation formula: Po, cp, X, 4′, 3a, 6″, 6C, 5S, 6‴, 2⁗; a ventral pore located outside the right side of the pore plate. The median anterior intercalary plate 2a pentagonal and the first precingular plate (1″) without contact to the first anterior intercalary plate (1a).

Holotype. SEM stub prepared from strain 35-R7 (designated CEDiT2020**H**115) deposited at the Senckenberg Research Institute and Natural History Museum, Centre of Excellence for Dinophyte Taxonomy (Wilhelmshaven, Germany).

Isotype. Formalin-fixed sample prepared from clonal strain 35-R7 (designated CEDiT2020**I**116) deposited at the

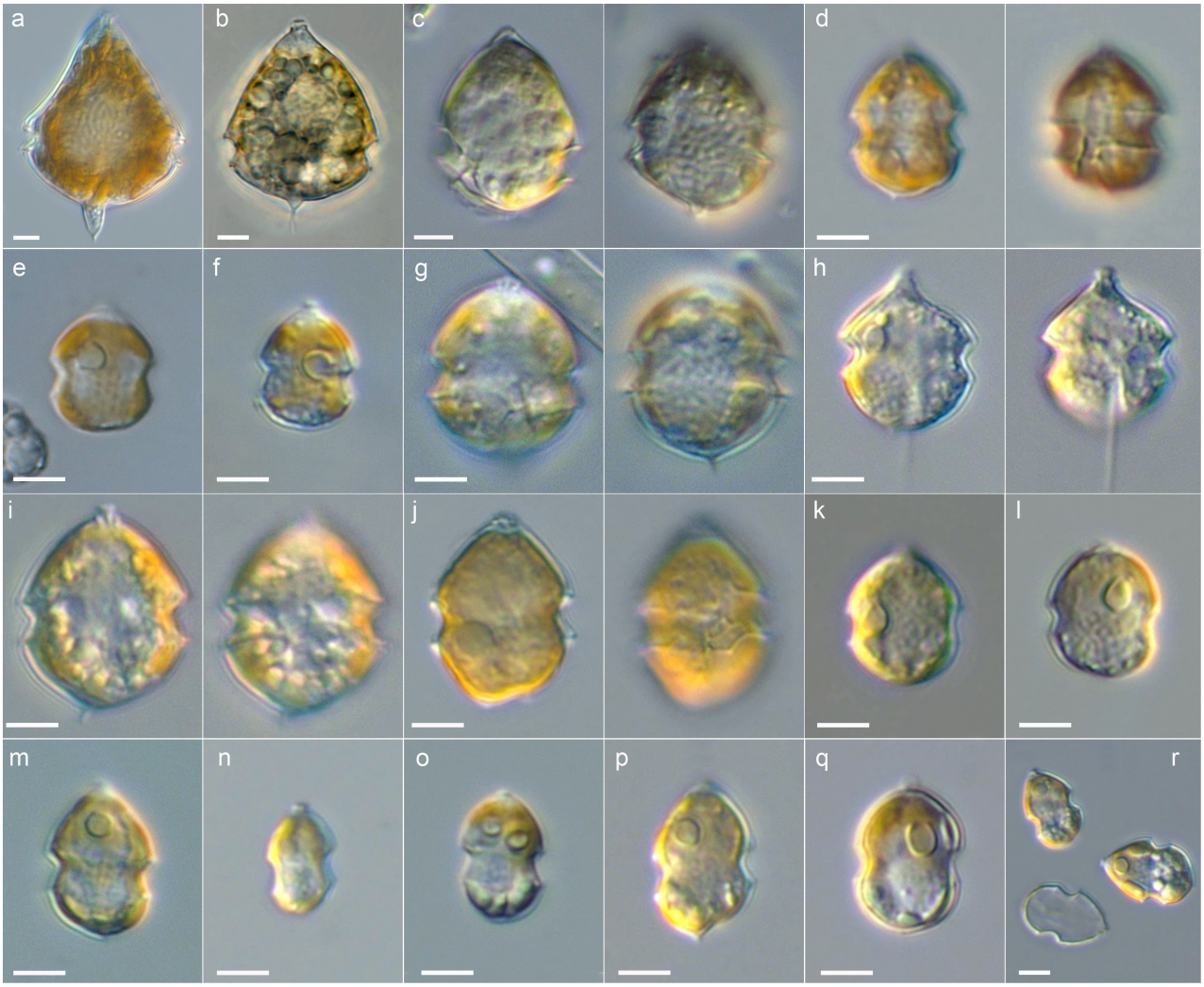

Fig 2. Diversity of Amphidomataceae in Irish waters as recorded in the oceanographic survey AZAHAB by live onboard light microcopy. (a) *Azadinium caudatum* var. *caudatum*. (b) *Az. caudatum* var. *margalefii*. (c) Two different focal planes of an unidentified *Azadinium* sp. (d) Two focal planes of *Az.* cf. *perfusorium*. (e, f) Two different cells of *Amphidoma languida*. (g) Two focal planes of *Az.* cf. *zhuanum*. (h) Two focal planes of a yet undescribed *Azadinium* sp. (*Azadinium* sp. 1). (i) Two different focal planes of an unidentified *Azadinium* species. (j) Two different focal planes of an unidentified *Azadinium* sp. (k, l) Two different cells of an unidentified amphidomatacean species. (m–o) Unidentified cells of *Azadinium* sp. (p–r) Different cells of *Azadinium* cf. *spinosum*. Scale bars: 5 μm. [Color figure can be viewed at wileyonlinelibrary.com]

Senckenberg Research Institute and Natural History Museum, Centre of Excellence for Dinophyte Taxonomy (Wilhelmshaven, Germany).

Type locality. North East Atlantic, West of Ireland (52°1.854′ N; 10°46.284′ W).

Etymology. The epithet galwayense honors the county of Galway in the west of Ireland where the first azaspiracid toxins were discovered from blue mussels grown in Killary Harbour in 1995 and where the Irish Marine Institute main laboratory is located.

All three strains of *Az. galwayense* obtained in the present study (35-R4, 35-R6, 35-R7) were identical in terms of morphology and plate pattern. Strain 35-R7 was selected to prepare the type material and is described in detail. Cells were small, ovoid in shape and slightly compressed ventrally. Newly formalin preserved cells range in size from 11.5–18.4 μm in length (mean length: 14.1 ± 1.3 μm; n = 47) and 8.5–15.1 μm in width (mean width: 10.6 ± 1.3 μm; n = 47) and a median length:width ratio of 1.34 ± 0.10 (Table 1). The cells had a dome shaped episome bearing a prominent apical pore complex (APC) (Fig. 3c, g). The hyposome had a rounded ending on an antapical spine (Fig. 3c). The cingulum was broad and deeply excavated, located in a post-median position and with a slight descending displacement from left to right in ventral view (Fig. 3d) of about one-third of the cingulum. A single chloroplast was visible and occupied the periphery of the cell (Fig. 3f, h). There was a single pyrenoid surrounded by a starch sheath in the left side of the episome (Fig. 3a, b). The nucleus with condensed and clearly visible chromosomes was large and round to ellipsoid and was sub-centrally located occupying a large part of the hyposome and a small part of the episome (Fig. 3c, f, h). Cells divided with an oblique

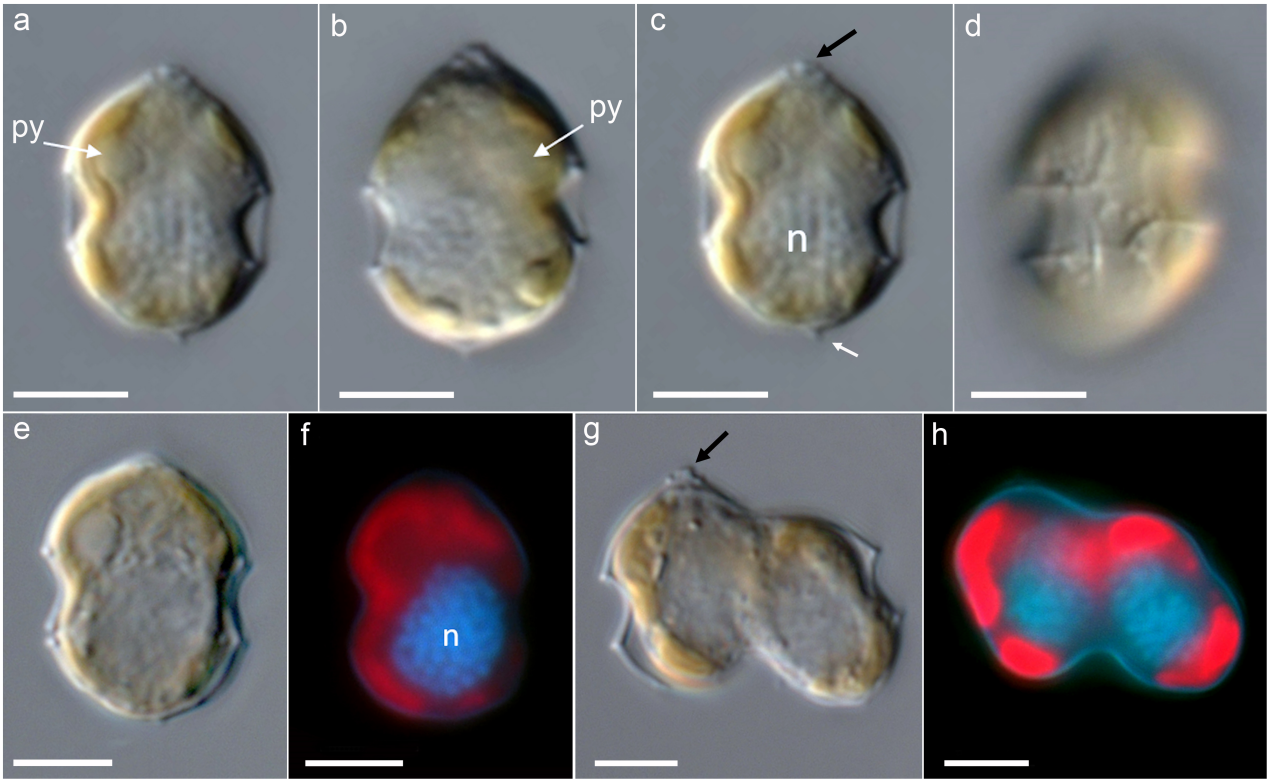

Fig 3. *Azadinium galwayense* sp. nov. (strain 35-R7). LM of formalin fixed cells. (a–d) General size and shape. Note the prominent apical pore complex (black arrow in c and g). (a, b) Arrow showing a pyrenoid (py) in the episome. (c) Nucleus (n) size and shape and antapical spine (white arrow). (d) Note the wide cingulum. (e–h) Formalin fixed cells stained with DAPI in brightfield (e) and with UV light excitation (f) to indicate shape, size and location of the nucleus (n) and the chloroplast. (g, h) Late stage of cell division (desmoschisis) in brightfield (g) and with UV light excitation (h). Scale bars: 5 μm. [Color figure can be viewed at wileyonlinelibrary.com]

fission line by desmoschisis, i.e. parent thecal plates were shared by the sister cells (Fig. 3g, h). No cyst formation was noticed in cultures.

Azadinium galwayense had the plate pattern Po, cp, X, 4′, 3a, 6″, 6C, 5S, 6‴, 2⁗ (Figs 4–6). The epitheca in apical view (Fig. 5a, b) showed a ventral pore (vp) in the right side of the APC, located between the 1′ and 4′ apical plate sutures and the pore plate (Po). The APC consisted of Po, a cover plate (cp) and X-plate (or canal plate). The Po were surrounded by a prominent and horse-shoe shaped rim (Fig. 5b). Four apical plates surrounded the APC. The 1′ apical plate was widest at the point where the sutures between 4′ and 6″ and 2′ and 1″ plates met ventrally and narrowed as it extended towards the sulcal area (Fig. 4a). Plates 2′ and 4′ were rhomboid in shape, and plate 3′ was small and hexagonal with very small sutures to the lateral apical plates 2′ and 4′ (Fig. 5a). The 1″ precingular plate was never in contact with the first intercalary plate (1a) (n = 50). The second intercalary plate (2a) was pentagonal and contacted both precingular plates 3″ and 4″ (Fig. 4b).

The cingulum was wide and excavated and consisted of six plates. Sutures of the cingular plates coincided with the sutures of the precingular plates (Fig. 4a, b). In lateral view (Fig. 5a, c), *Az. galwayense* was slightly dorso-ventrally flattened. The sulcal area consisted of five sulcal plates (Fig. 5d). The anterior sulcal plate (Sa) was large, rectangular, occupied a large part of the cingular area, and was in touch with the first and sixth cingular plates, and extended slightly into the epitheca. The posterior sulcal plate (Sp) extended about two-thirds the distance from the cingulum to the antapex. The left sulcal plate (Ss) was broad, anteriorly located to the Sp and running transversally from plate C1 to C6. The central sulcal area was made of two smaller sulcal plates Sm and Sd (Fig. 5d, Fig. S1 in the Supporting Information).

The hyposome consisted of six post-cingular and two antapical plates. Plates 3‴ and 5‴ were the widest and 1‴ was the narrowest. The 2⁗ plate was the largest of the two antapical plates and the one bearing a conspicuous spine.

The thecal plates were smooth and thecal pores of slightly varying diameter (range 0.09–0.16 μm, mean 0.12 ± 0.02 μm, n = 20) were found scattered on many plates (Figs 4–6, Fig. S1 in the Supporting Information). Thecal pores were found in varying numbers and positions in plates of the both the epitheca and hypotheca and were most conspicuous in the four apical plates and in the 1a and 3a intercalary plates. Plate 2a was consistently free of pores (Figs 4b, 5a). Long rows of almost evenly spaced thecal pores were present in the cingular plates along the episome boundary (Fig. 4a, b). On the hypothecal plates the pores were positioned closer to the sutures with other plates, and they were especially bunched

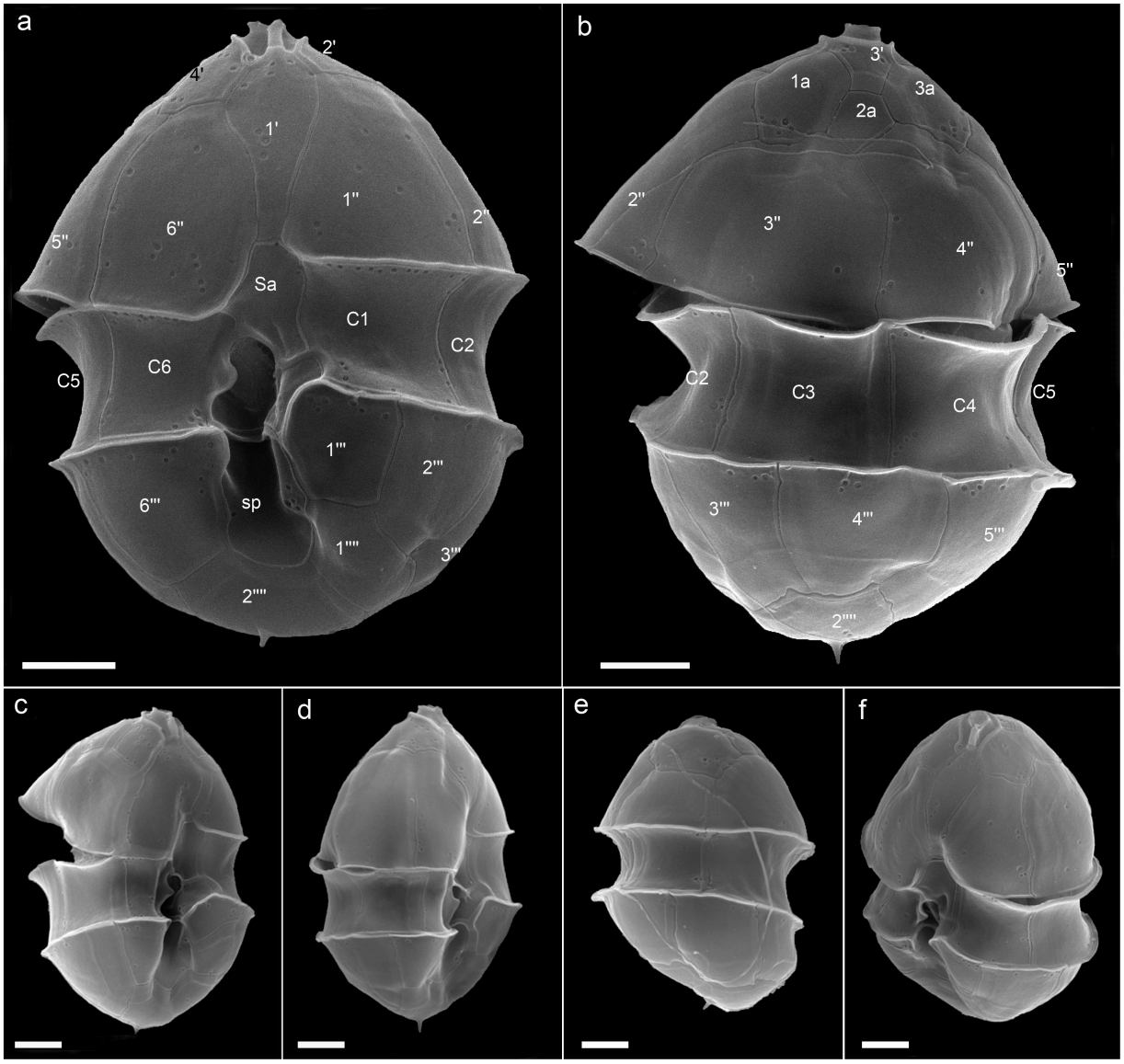

Fig 4. *Azadinium galwayense* sp. nov. (strain 35-R7). SEM micrographs of different thecae in (a) ventral and (b) dorsal view. (c–f) Lateral views. Scale bars: 2μm.

together around the spine in the 2′′′′ (Fig. 5c) and dorsally positioned to the spine.

Azadinium perfusorium Tillmann & Salas sp. nov.
Figures 7–10, Figures S2–S5 in the Supporting Information

Description. Small photosynthetic thecate Dinophyceae; cells 11.4 to 18.0 μm long and 8.3 to 13.5 μm wide; cingulum broad and median; epitheca conical and ending in a small but distinctly pointed apical pore; hypotheca hemispherical with a very broad and long sulcus and with a single antapical spine; tabulation formula: Po, cp, X, 4′, 3a, 6′′, 6C, 5S, 6′′′, 2′′′′; a ventral pore located on the right ventral side of the pore plate at the junction of apical plates 1′ and 4′. Apical plate 4′ larger and extend more ventrally than apical plate 2′. Anterior intercalary plates 1a and 3a large and plate 2a small and tetragonal.

Holotype. SEM stub (designated CEDiT2020**H**117) prepared from strain 5-B8 deposited at the Senckenberg Research Institute and Natural History Museum, Centre of Excellence for Dinophyte Taxonomy (Wilhelmshaven, Germany).

Isotype. Formalin-fixed sample prepared from clonal strain 5-B8 (designated CEDiT2020**I**118) deposited at the Senckenberg Research Institute and Natural History Museum, Centre of Excellence for Dinophyte Taxonomy (Wilhelmshaven, Germany).

Type locality. North East Atlantic, West of Ireland (52°1.854′ N; 10°46.284′ W).

Etymology. The epithet (Latin, *perfusorius*: superficial, cursory) is inspired by the almost identical light microscopy appearance of this species and *Azadinium dalianense* Z.Luo,

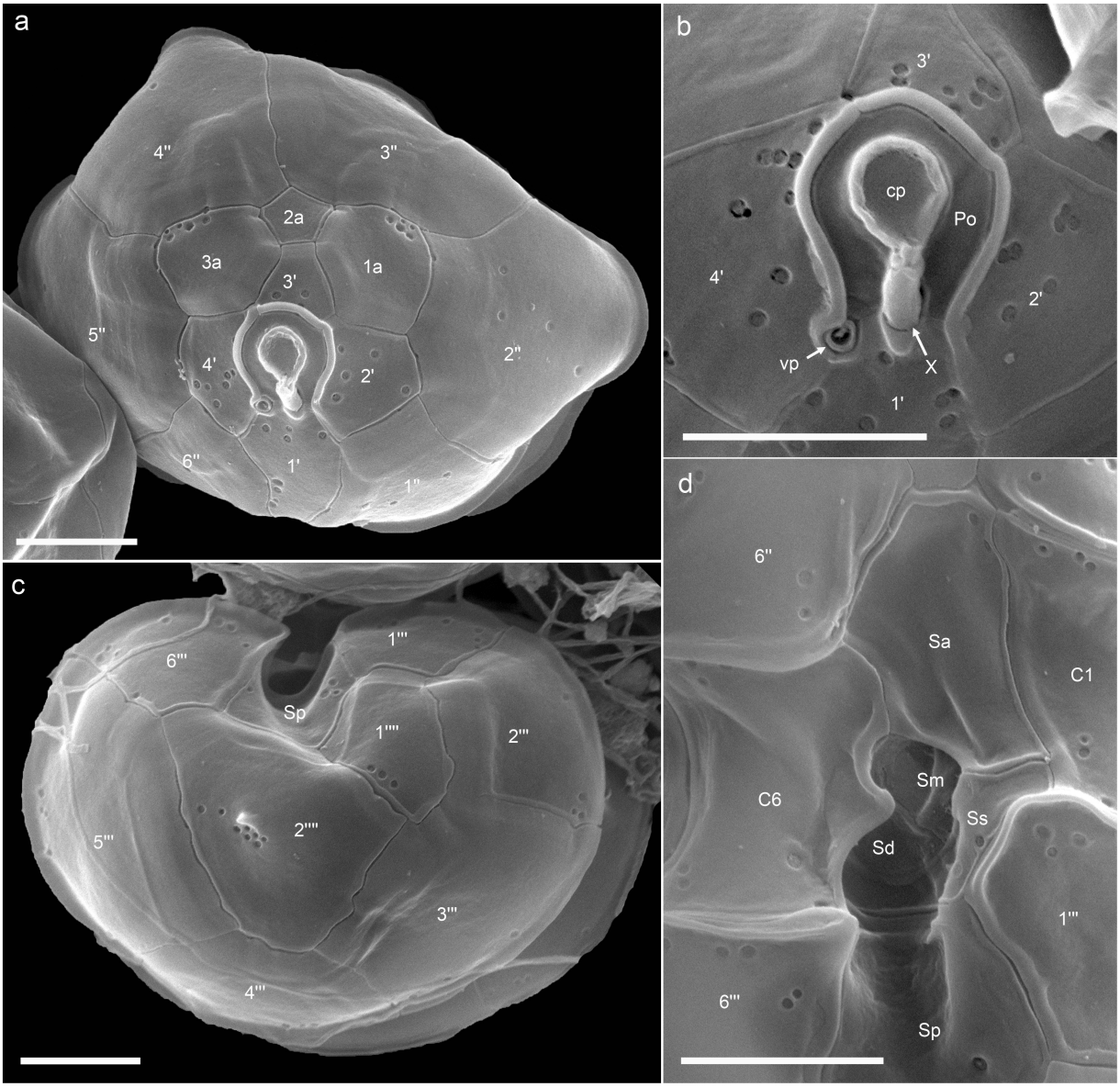

Fig 5. *Azadinium galwayense* sp. nov. (strain 35-R7). SEM micrographs of different thecae. (a) Epithecal plates in apical view. (b) Detailed view of the apical pore complex (APC). Note the position of the ventral pore (vp). (c) Hypothecal plates in antapical view. (d) Detailed view of the sulcal plates. cp, cover plate; Po, pore plate; Sa, anterior sulcal plate; Sp, posterior sulcal plate; Ss, left sulcal plate; Sm, median sulcal plate; Sd, right sulcal plate; X, X-plate. Scale bars: 2μm.

H.Gu & Tillmann (antapical spine, pyrenoid located in the hyposome), such that the field sample specimens initially (and obviously cursory) were misidentified as *Az. dalianense*.

All 25 strains identified as *Az. perfusorium* were inspected with LM (Table 1) and were identical in size, shape, presence of antapical spine, and presence and position of the pyrenoid. A selected number of strains inspected by SEM revealed all other morphological details as being identical as well. Cells of strain 5-B8, from which the holotype was prepared, is described and depicted in detail. Cells of *Az. perfusorium* strain 5-B8 ranged in size from 12.9–15.7 μm in length (mean length: 14.2 ± 0.7μm; n = 53) and 9.3–12.0 μm width (mean width: 10.7 ± 0.7 μm; n = 53). They had a length:width ratio of 1.33 ± 0.05 and were not dorso-ventrally compressed (i.e. almost circular in apical view). Cells were ovoid in outline and had a dome shaped episome and a rounded hyposome (Fig. 7). The cingulum was wide and excavated, slightly post-median in position, and descending with a slight displacement of about 1/3 of the cingulum width (Fig. 7f). A single chloroplast was reticulate and parietally arranged (Fig. 7f, g). A single large pyrenoid visible by a starch sheath was invariably located on the right side of the hyposome (Fig. 7b, c, d, e). The nucleus was round to slightly ovoid and almost centrally located (Fig. 7h, i, j). Cells divided by desmoschisis with an oblique fission line (Fig. S2j–n in the Supporting Information). No cyst formation was noticed in cultures.

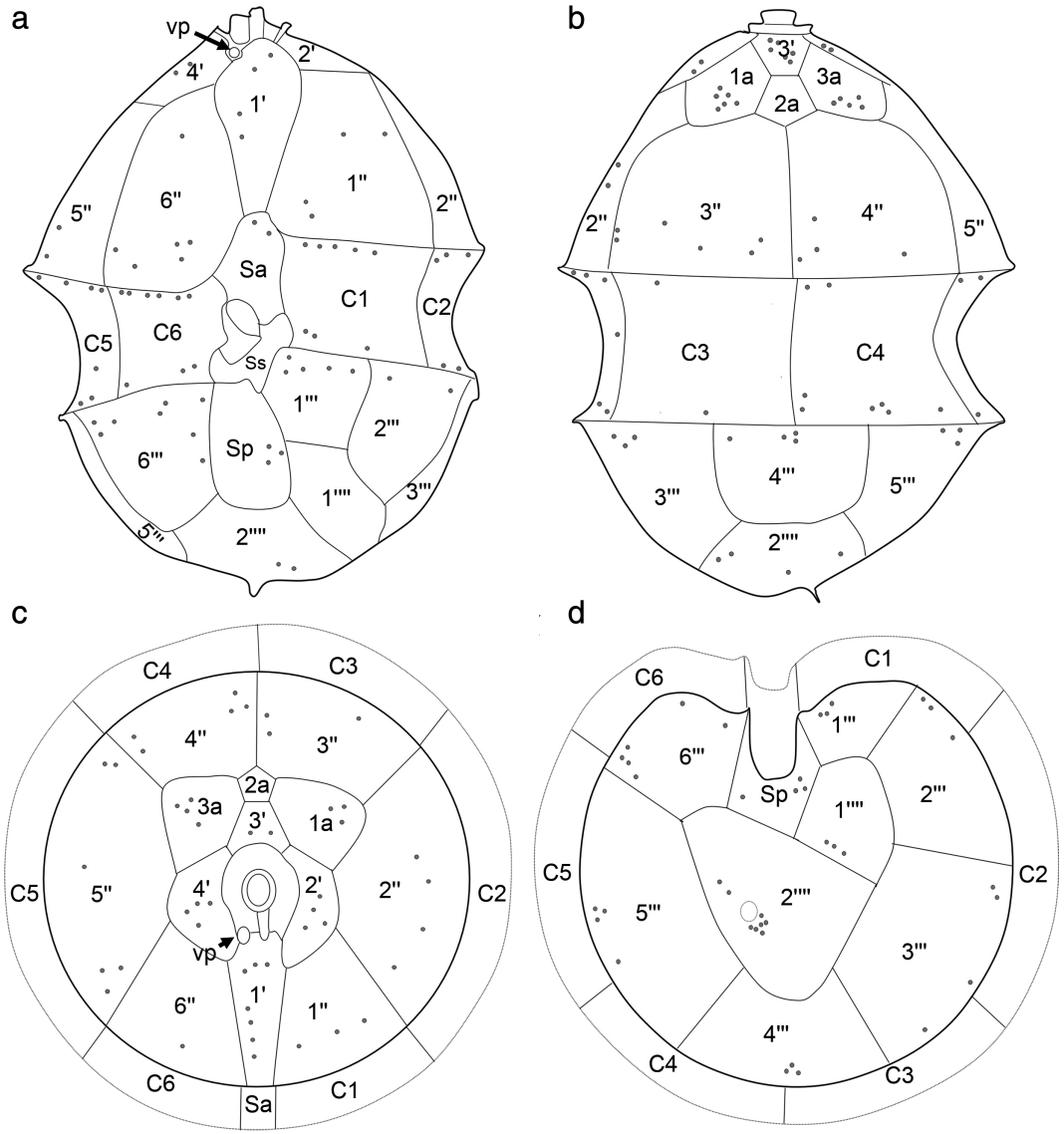

Fig 6. *Azadinium galwayense* sp. nov. (strain 35-R7). Schematic illustration of thecal plates. (a) Ventral view. (b) Dorsal view. (c) Apical view. (d) Antapical view. Plate labels according to the Kofoidian system. Abbreviations of sulcal plates: Sa, anterior sulcal plate; Sp, posterior sulcal plate; Ss, left sulcal plate.

SEM revealed the thecal plate pattern (Po, cp, X, 4′, 3a, 6″, 6C, 5S, 6‴, 2⁗) and other thecal plate details (Figs 8–10, 10, Figs S2–S5 in the Supporting Information). In the epitheca there were four apical plates and six precingular plates. The APC had a horseshoe shape and consisted of Po, cp and an X-plate (Fig. 9a–c). The Po had an obvious raised surrounding rim which was formed by the lateral and dorsal apical plates and which was open ventrally (Fig. 9a, c). A small X-plate was located centrally between plates 1′ and Po and its outer structure was connected with the cp through a finger-like protrusion (Fig. 9c). The vp was located on the right ventral end of Po at the junction of plates 1′ and 4′ (Fig. 9a, c). The four apical plates were quite different in shape and size. The ventral 1′ plate was wide anteriorly and narrowed towards the anterior sulcal plate (Fig. 8a). Apical plates 2′ and 4′ were small and pentagonal (plate 2′) or hexagonal (plate 4′). Both lateral apical plates had a very short suture with the hexagonal dorsal apical plate 3′. Plate 4′ was distinctly asymmetrical in shape and extended more lateral than plate 2′ into the ventral area (Fig. 9a).

Among the series of three anterior intercalary plates both lateral plates 1a and 3a had a large size. The central anterior intercalary plate 2a was much smaller and tetragonal in shape and symmetrically located above precingular plate 3″ (Figs 8b, 9a). The first anterior intercalary plate 1a was always in contact with the ventrally located precingular plate (1″) whereas plate 3a on the cell's right side was disconnected from the ventral precingular plate 6″ by the lanceolate end of plate 4′ (Fig. 9a).

The cingulum with small lists on both sides consisted of six cingular plates (Fig. 9e) which were lined up in position with the precingular plates. In the sulcal area there were five

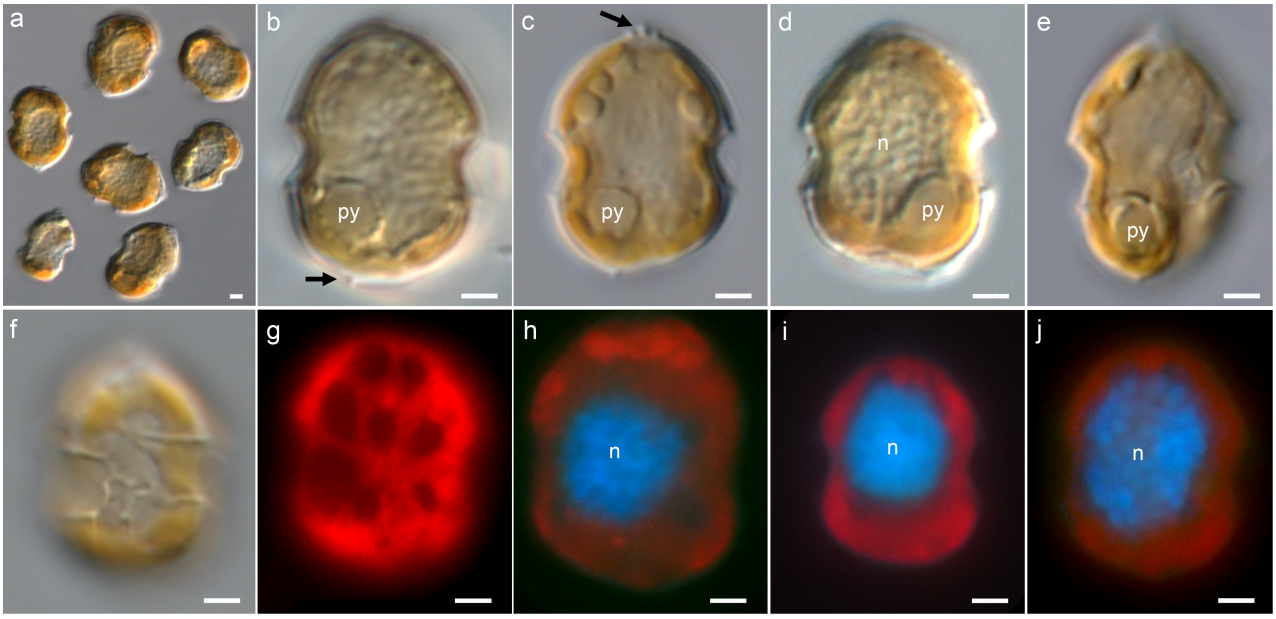

Fig 7. *Azadinium perfusorium* sp. nov. (strain 5-B8). LM of formalin fixed cells. (a–f) General size and shape. Note the pyrenoid (py) located in the hyposome, the antapical spine (black arrow in b) and the prominent apical pore complex (black arrow in c). (d) Nucleus (n) size and position. (e) Cell in lateral view. (f) Ventral view, note the wide cingulum. (g) Cell with blue light excitation showing the reticulate chloroplast. (h–j) Formalin fixed and DAPI stained cells with UV light excitation to indicate shape, size and location of the nucleus (n). Scale bars: 2 μm. [Color figure can be viewed at wileyonlinelibrary.com]

sulcal plates (Fig. 9e, g). The anterior sulcal plate (Sa) was narrow, and extended into the epitheca, whereas the posterior sulcal plate (Sp) was wide and extended into the hypotheca (Fig. 8a). Below the Sa, a left sulcal plate (Ss) extended across the sulcal area from C1 to C6 (Fig. 9f, g). Two small plates (Sm and Sd) formed a concave shaped vaulted center and were surrounded by Sa, Ss and C6 (Fig. 9f, g).

The hypotheca consisted of six postcingular and two antapical plates (Fig. 9d). The large and hexagonal plate 2‴ bore a single antapical spine which was in a ventral position close to the Sp plate (Fig. 9d). The 1‴ plate was smaller and pentagonal in shape (Fig. 9d).

The thecal plates were smooth and thecal pores were sparsely scattered around the plates (Figs 7–9). Thecal pores ranged in diameter from 0.09 to 0.16 μm (mean: 0.11 ± 0.02 μm, n = 20). Plate 2a was consistently free of thecal pores (Figs 8b, 9a). On the hypotheca, thecal pores on postcingular plates were positioned closer to the cingulum. A cluster of pores was located on the dorsal side of plate 2‴ distant from the antapical spine (Fig. 9d) which was situated on a more ventral position and closer to the posterior sulcal plate.

Other species

Next to these two new species, one strain was designated as *Az.* cf. *zhuanum*. This is the first strain close to or conspecific with *Az. zhuanum* from North Atlantic waters. As this strain differed in morphology from the strain on which *Az. zhuanum* was originally described, we here present a detailed morphological analysis. Cells of strain 32-R1 were small, round to ovoid in shape and slightly compressed ventrally. Cells ranged in size from 14.9–20.1 μm in length (mean length: 17.2 ± 1.2 μm; n = 49) and 12.3–17.5 μm in width (mean width: 14.2 ± 1.3 μm; n = 49) and had a median length: width ratio of 1.21 ± 0.07 (Table 1). The cells' episome was conical bearing a prominent apical pore complex (APC) (Fig. 11a, e). The hyposome was hemispherical bearing a long and robust antapical spine (Fig. 11c, d, h). The cingulum was broad and deeply excavated, post median and slightly offset of about one-third of the cingulum width (Fig. 11b).

A single chloroplast was parietally arranged around the periphery of the cell (Fig. 11j). There was a single pyrenoid surrounded by a starch sheath and this could be positioned in the episome left side or hyposome right side (Fig. 11e–g). Exceptionally, cells with two pyrenoids were also recorded (Fig. 11h). The round nucleus with clearly visible chromosomes was located in the hyposome (Fig. 11k, l), but – presumably during early nuclear division – an enlarged and centrally located nucleus was observed (Fig. 11h). During cell division the nucleus was elongated in an anterior/posterior axis occupying part of the episome (Fig. 11m, o). Cells divided by desmoschisis with an oblique fission line (Fig. 11n).

The dominant thecal plate pattern of *Az.* cf. *zhuanum* strain 32-R1 was Po, cp, X, 3′, 2a, 6″, 6C, 5S, 6‴, 2‴ (Figs 11p–r, 12, 13, Fig. S6 in the Supporting Information). The epitheca in apical view (Fig. 12a, d) revealed the location of the ventral pore inside the right side of the pore plate. The APC consisted of Po, a cover plate (cp), and the X-plate (or canal plate) (Fig. 12d). The Po was surrounded by a prominent horse-shoe shaped rim (Fig. 12a, e). Three apical plates surrounded the APC. The 1′ plate was long and narrow, somewhat rectangular in shape (Figs 11p, q, 12a, b). Plate 2′ extended from the Po on the left side ventrally all the way around the Po to a mid to right-dorsal position. The 3′ plate

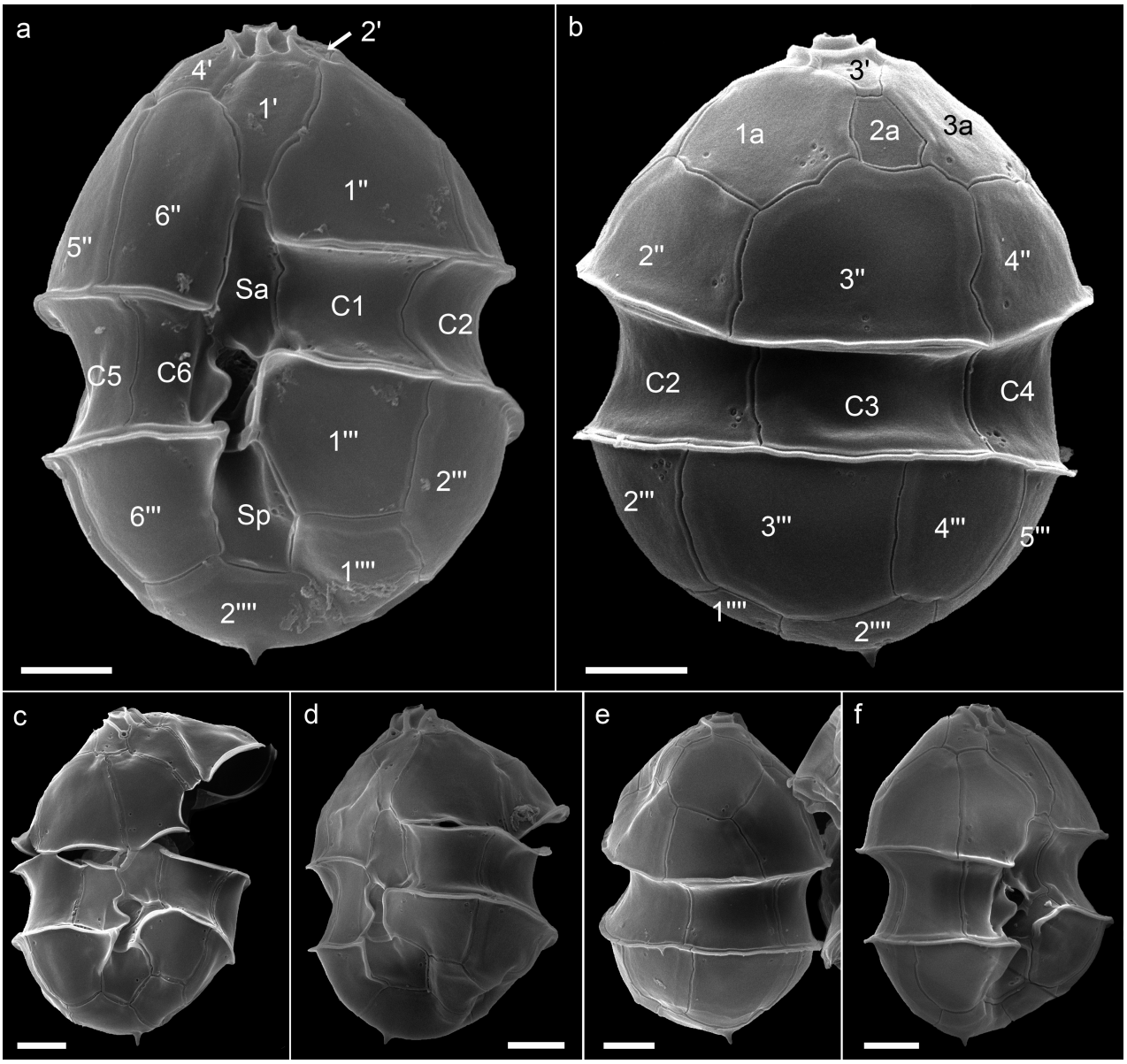

Fig 8. *Azadinium perfusorium* sp. nov. (strain 5-B8). SEM micrographs of different cells in (a) ventral and (b) dorsal view. (c) Ventral view. (d) Left lateral - ventral view. (e) Right lateral view. (f) Right lateral - ventral view. Scale bars: 2 μm.

was five-sided in shape (Fig. 12a, b, d). The anterior intercalary plates were located in a dorsal position with the suture between the 1a and 2a generally in a mid-dorsal position and in contact with the 2′ plate. The 1a plate was generally larger than the 2a plate and pentagonal in shape and not in contact with plate 3′. In contrast, the 2a was quadrangular and straddles between the 2′ and 3′ plates (Fig. 12a, b).

The precingular plates were roughly of similar size except for the 5″ plate which was slightly larger (Fig. 12a, b), the mid-dorsal 3″ plate was the only precingular plate in contact with all intercalary plates.

The cingulum was wide and excavated and consisted of six plates (Fig. 11p, q). The sulcal area consisted of five plates (Fig. 12g). The anterior sulcal (Sa) was large and extended slightly into the epitheca. The left sulcal (Ss) was located below the Sa and extended across from C1 to C6 in a slightly downward trajectory. The median sulcal (Sm) and right sulcal (Sd) were located in the sulcal central area and were the smallest of the series (Fig. 12g). The posterior sulcal (Sp) plate below the Ss extended into the hypotheca half to two-thirds of the hypothecal length and was pentagonal in shape (Fig. 11p, q).

The hypotheca consisted of six postcingular plates and two antapical plates (Fig. 12f). The 2′′′′ plate was the largest of the two antapical plates and the one bearing a large conspicuous spine. The spine was quite robust and supported by ridges and several pores were clustered around its base.

The thecal plates were smooth and scattered by thecal pores of slightly varying size with pore diameter varying between 0.09 and 0.14 μm (mean: 0.12 ± 0.01, n = 20).

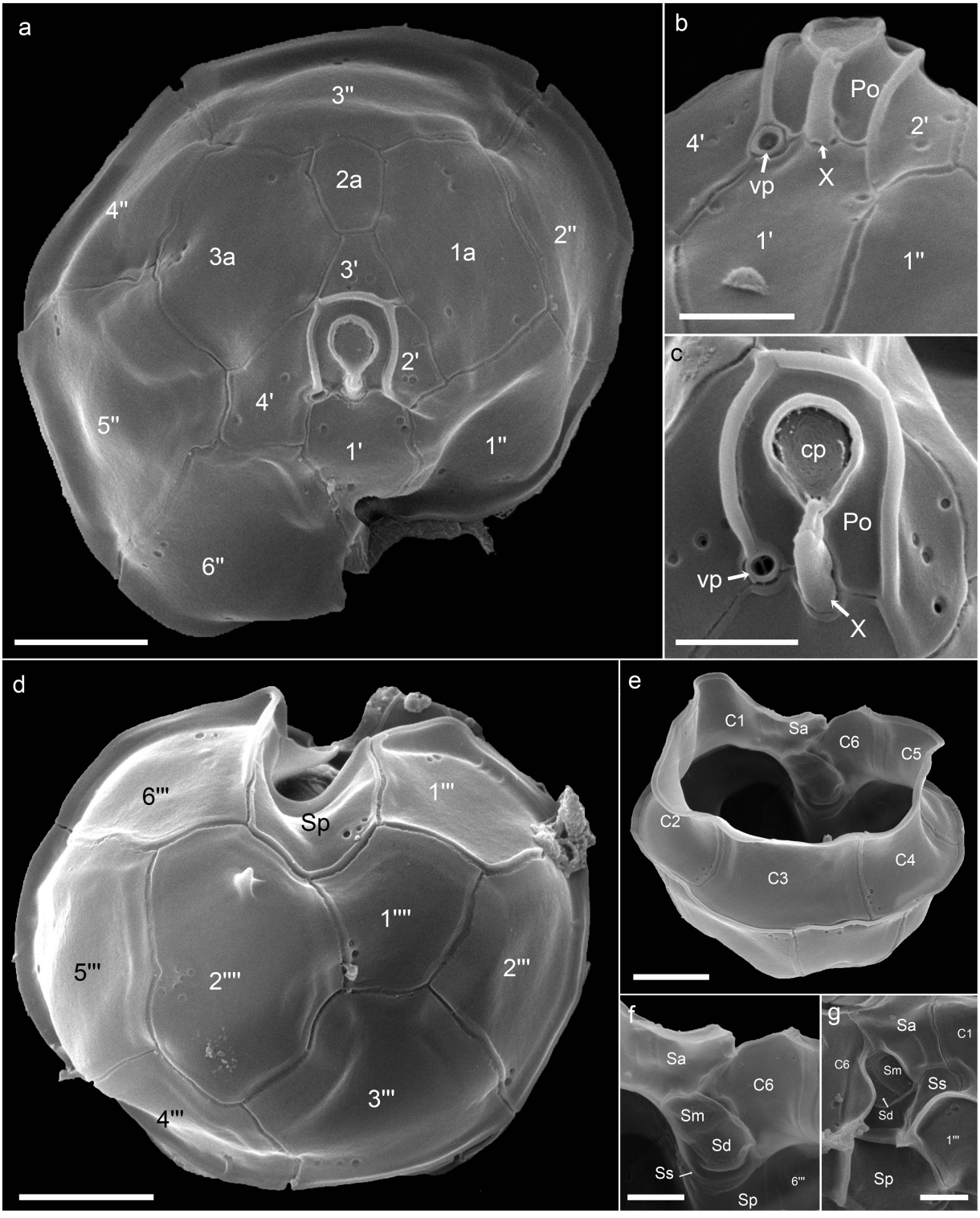

Fig 9. *Azadinium perfusorium* sp. nov. (strain 5-B8). SEM micrographs of different thecae. (a) Epithecal plates in apical view. (b, c) Detailed view of the apical pore complex (APC) in (b) ventral or (c) apical view. Note the position of the ventral pore (vp). (d) Hypothecal plates in antapical view. (e) Hypotheca in apical-dorsal view showing cingular plates. (f, g) Detailed view of sulcal plates in internal (f) or outside (g) view. cp, cover plate; Po, pore plate; Sa, anterior sulcal plate; Sp, posterior sulcal plate; Ss, left sulcal plate; Sm, median sulcal plate; Sd, right sulcal plate; X, X-plate. Scale bars: 2 μm (a, d, e) and 1 μm (b, c, f, g).

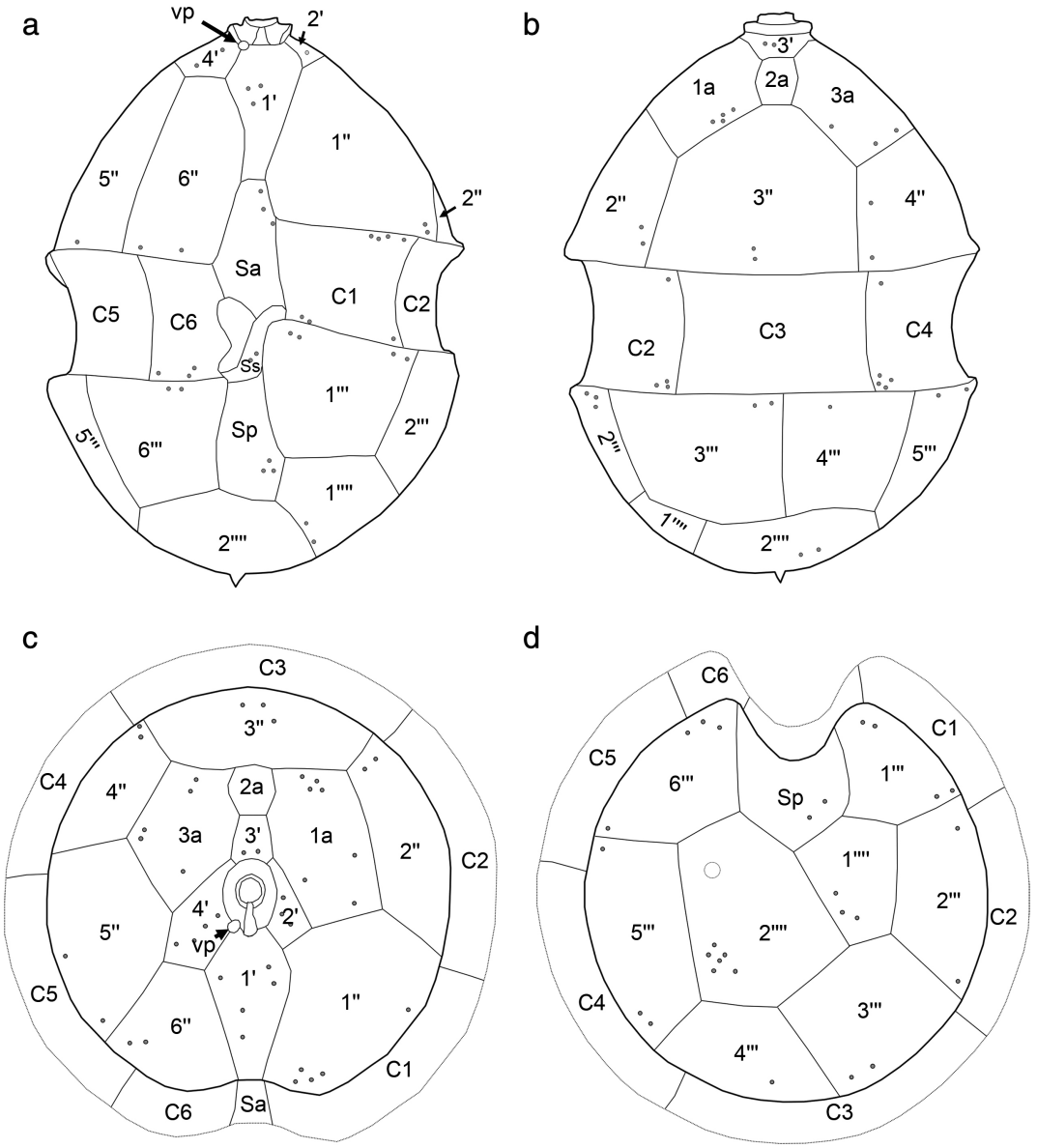

Fig 10. *Azadinium perfusorium* sp. nov. (strain 5-B8). Schematic illustration of thecal plates. (a) Ventral view. (b) Dorsal view. (c) Apical view. (d) Antapical view. Plate labels according to the Kofoidian system. Abbreviations of sulcal plates: Sa, anterior sulcal plate; Sp, posterior sulcal plate; Ss, left sulcal plate.

Pores were most prominent in the apical series (Fig. 12d) and in the antapical plates (Fig. 12f), where several pores were characteristically scattered around the base of the spine.

In the cultured material of strain 32-R1, deviations from the dominant plate pattern described above were regularly encountered. Variability in the number of plates was most obvious for epithecal plates (Figs 12h, Fig. S7 in the Supporting Information). To quantitatively estimate the number of plates in apical and anterior intercalary plate series, a SEM stub was systematically scanned, and the number of plates in each series was scored for cells, in which all plates of a series were visible. This procedure was performed twice in Ireland and Germany for independently grown cultures in late exponential growth phase. Both quantifications of epithecal plates yielded similar results (Table 2). Overall, 85% of all cells had three apical plates, whereas for 15% of cells four apical plates were present. The dominant combination of three apical and two anterior intercalary plates were present for 70% of cells. Deviating numbers of precingular, postcingular or antapical plates were rarely observed as well but were not quantified.

A single strain of *Az. caudatum* var. *margalefii* (9-E13) was obtained during this survey from station 20. Both varieties, var. *margalefii* and var. *caudatum*, were identified in plankton samples (Fig. 2) but only this variety survived in culture (Fig. 14). The size was 28.5 ± 2.4 μm in length and 22.8 ± 2.3 μm in width (Table 1). Plate pattern and arrangement (Fig. 14f–k) was identical to the description of Nézan *et al*. (2012).

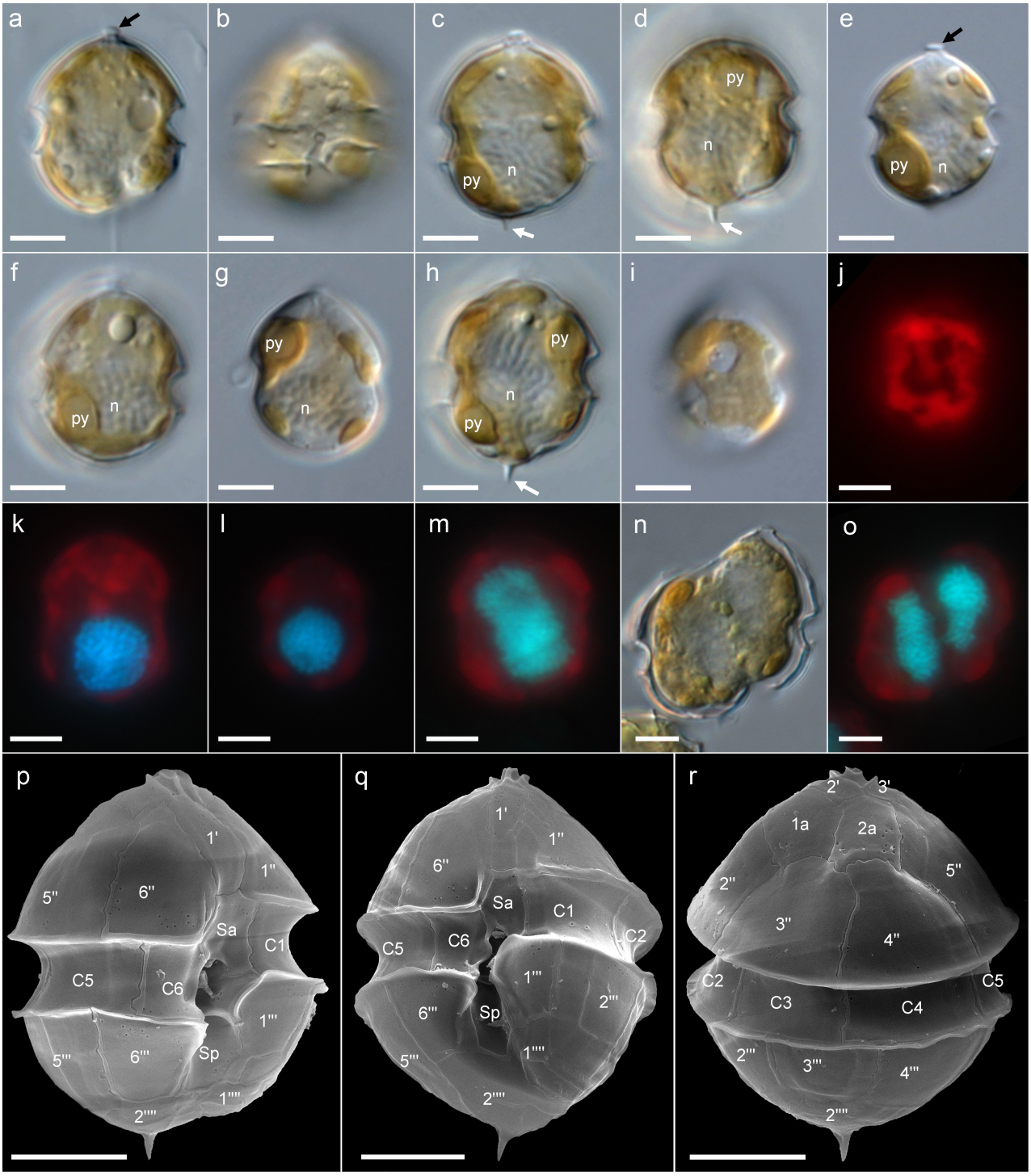

Fig 11. *Azadinium* cf. *zhuanum* (strain 32-R1). LM of living (a–i) or formaldehyde fixed cells (j–o), or SEM images (p–r). (a–i) General size and shape. Note the broad cingulum (b), the prominent apical pore complex (black arrows in a, e), and the prominent antapical spine (white arrows in c, d, h). (c–g) Position of pyrenoid (py) either in the episome (d, g) or hyposome (c, e, f). (h) Cell (presumably in early stage of cell division) with two pyrenoids and an elongated and centrally located nucleus. (i) Note the parietally arranged and reticulate chloroplast. (j) Formaldehyde fixed cells viewed with blue light excitation to indicate shape of the chloroplast. (k–m) DAPI stained cells observed under UV light excitation showing position, shape and size of the nucleus. (m) Cell in early stage of cell division, note the elongated nucleus. (n, o) Late stage of cell division (desmoschisis) in brightfield (n) and with UV light excitation (o). (p–r) SEM of different theca in (p) right lateral view, (q) ventral view, and (r) dorsal view. Scale bars: 5 μm. [Color figure can be viewed at wileyonlinelibrary.com]

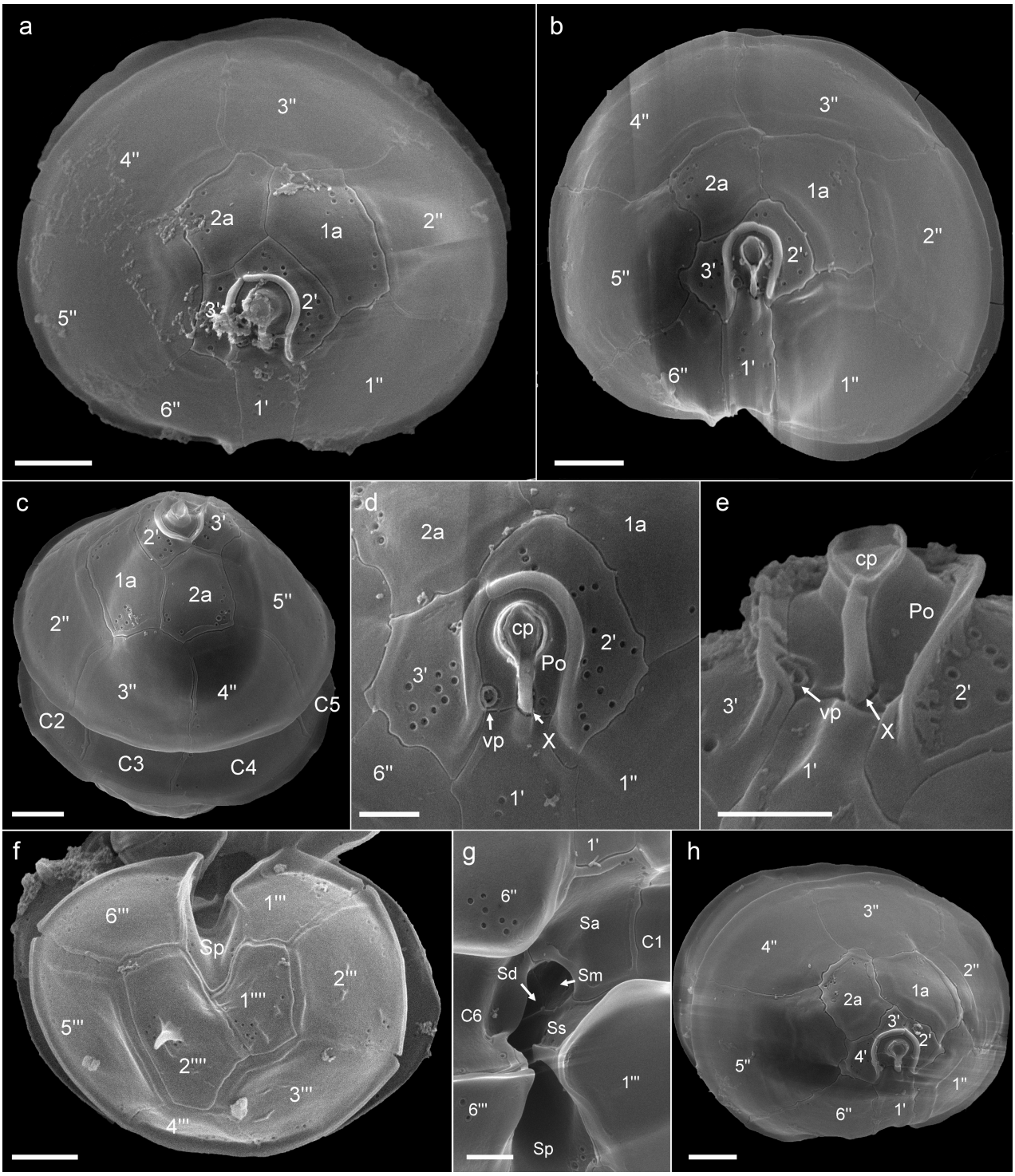

Fig 12. *Azadinium* cf. *zhuanum* (strain 32-R1). SEM images of different thecae. (a, b) Epithecal plates in apical view. (c) Epitheca in dorsal view. (d, e) Detailed view of the apical pore complex (APC) in apical (d) and ventral (e) view. Note the position of the ventral pore (vp). (f) Hypothecal plates in antapical view. (g) Detailed view of sulcal plates. (h) Apical view of epithecal plates showing a deviating plate pattern with four apical plates. cp, cover plate; Po, pore plate; Sa, anterior sulcal plate; Sp, posterior sulcal plate; Ss, left sulcal plate; Sm, median sulcal plate; Sd, right sulcal plate; X, X-plate. Scale bars: 2 μm (a–c, f, h) and 1 μm (d, e, g).

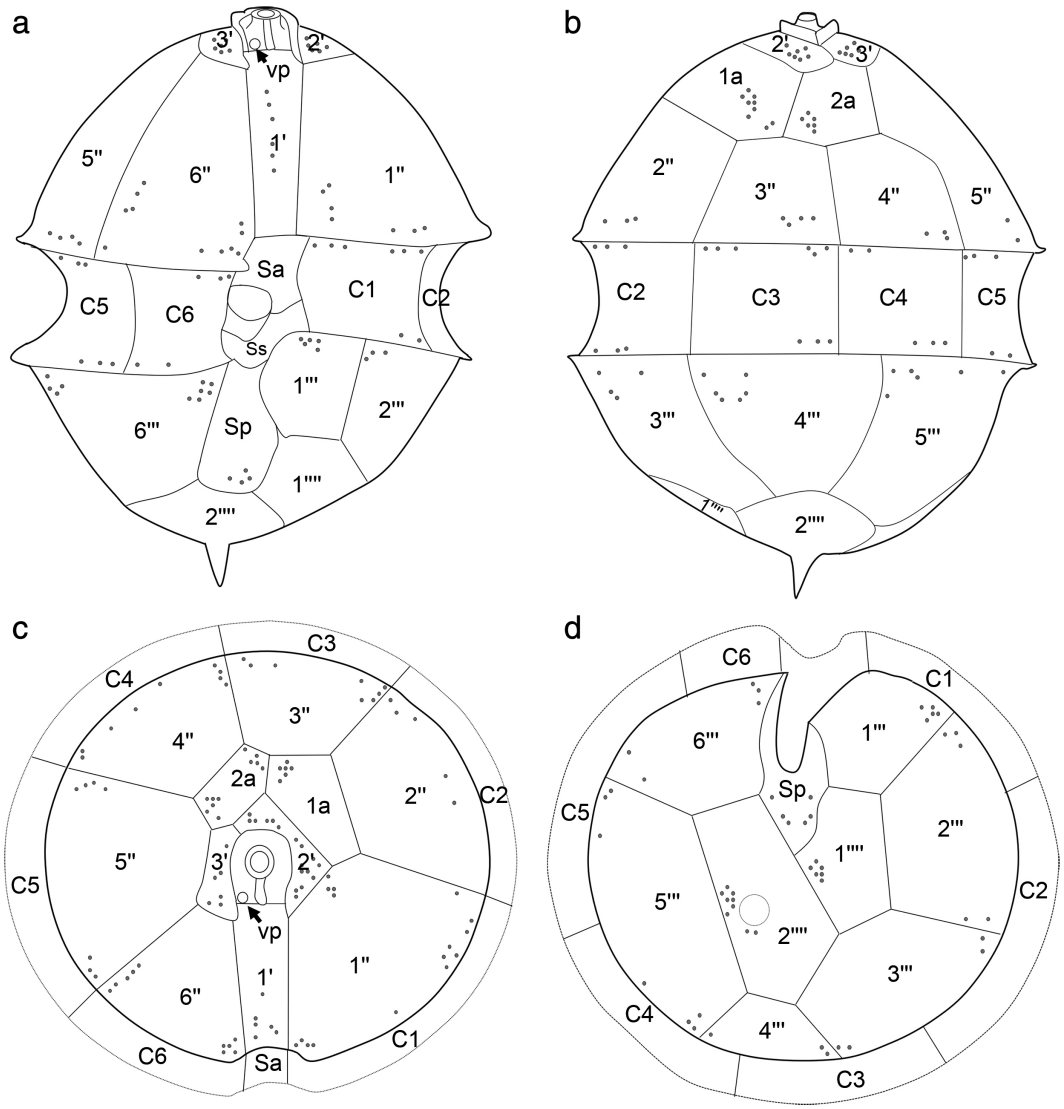

Fig 13. *Azadinium* cf. *zhuanum* (strain 32-R1). Schematic illustration of thecal plates. (a) Ventral view. (b) Dorsal view. (c) Apical view. (d) Antapical view. Plate labels according to the Kofoidian system. Abbreviations of sulcal plates: Sa, anterior sulcal plate; Sp, posterior sulcal plate; Ss, left sulcal plate.

Table 2. % quantification of apical and anterior intercalary plates per cell for *Azadinium* cf. *zhuanum* strain 32-R1 grown in Ireland (Q1) or Germany (Q2). The dominant plate pattern of three apical and two intercalary plates is highlighted in grey

Number of apical plates	3			4			
Number of intercalary plates	1	2	3	1	2	3	n
Q1	14.5%	62.0%	3.6%	3.6%	14.5%	1.8%	55
Q2	8.0%	75.0%	5.0%	1.0%	11.0%	0%	100
Overall	**10.3%**	**70.4%**	**4.5%**	**1.9%**	**12.2%**	**0.6%**	155

Azaspiracid analysis

All strains were negative for AZA. The limits of detection (LOD) in the SRM mode for the targeted analysis of known AZA for the three highest biomass samples was 0.001 fg cell^{-1} for *Az. galwayense* and *Az. perfusorium*, and 0.003 and 0.174 fg cell^{-1} for *Az.* cf. *zhuanum* strain 32-R1 and *Az. caudatum* var. *margalefii* strain 9-E13, respectively (Table S1 in the Supporting Information). All LOD data including LOD in the less sensitive precursor ion mode for the search of unknown AZA variants are listed in Table S2 in the Supporting Information.

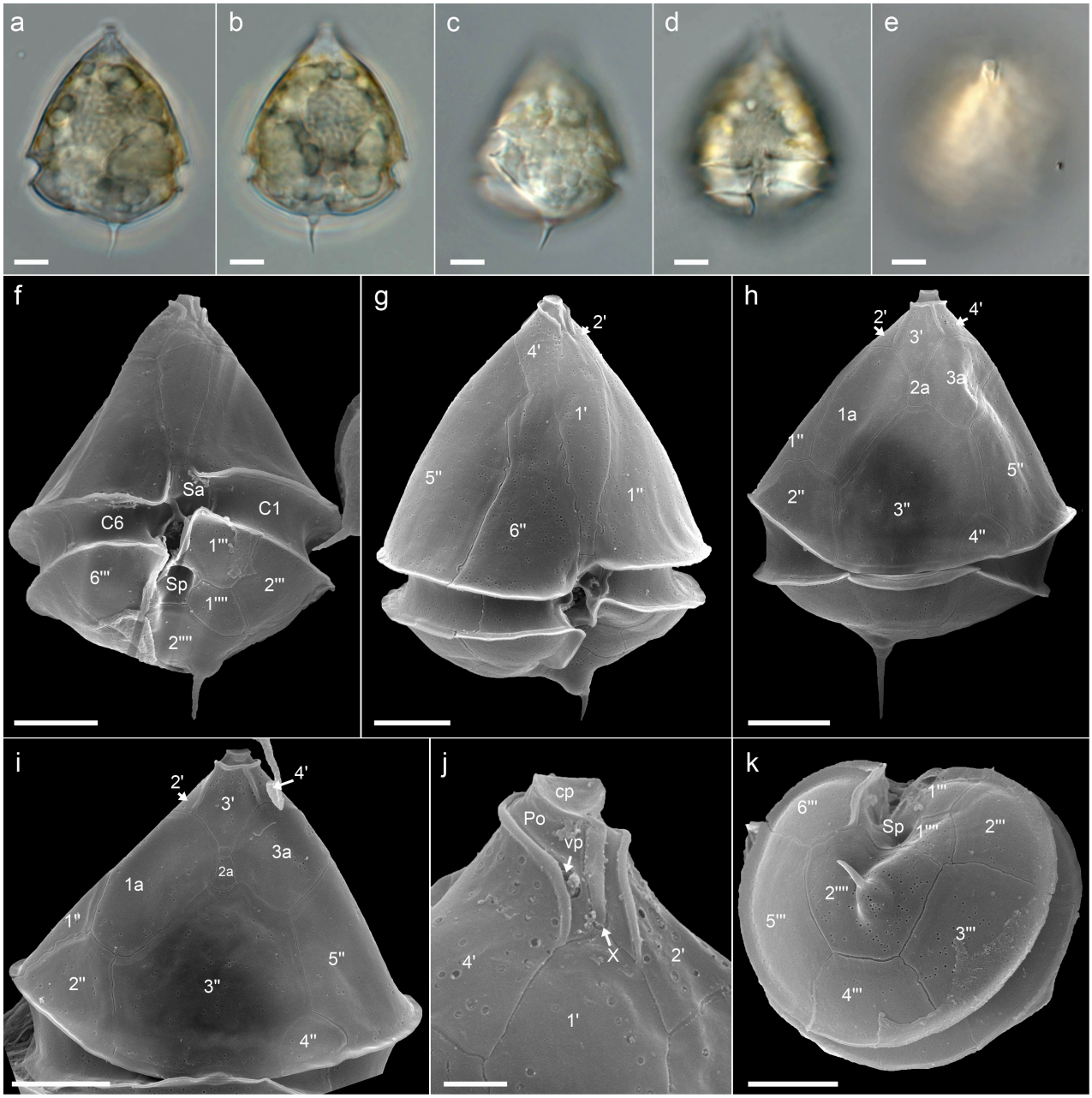

Fig 14. *Azadinium caudatum* var. *margalefii* (strain 9-E13). LM of living cells (a–e) and SEM images (f–k). (a–e) General size and shape. (f–h) SEM of whole theca in (f, g) ventral or (h) dorsal view. (i) Epithecal plates in dorsal view. (j) Detailed ventral view of the apical pore complex (APC). (k) Hypothecal plates in antapical view. cp, cover plate; Po, pore plate; Sa, anterior sulcal plate; Sp, posterior sulcal plate; vp, ventral pore; X, X-plate. Scale bars: 5 μm (a–i, k) and 1 μm (j). [Color figure can be viewed at wileyonlinelibrary.com]

Sequence divergences and molecular phylogeny

For SSU rRNA gene sequences comparison, all three strains of *Az. perfusorium* (5-B8, 2-D1, 6-B4) selected for SSU sequencing shared identical sequences, and three strains of *Az. galwayense* (35-R4, 35-R6, 35-R7) shared 99.9% similarity. *Azadinium perfusorium* shared 99.4% similarity with *Az. galwayense*.

For LSU rRNA gene sequences comparison, all three strains of *Az. galwayense* (35-R4, 35-R6, 35-R7) shared identical sequences. All 11 strains of *Az. perfusorium* selected for LSU sequencing shared identical sequences, too. *Azadinium galwayense* shared 95.0% similarity with *Az. perfusorium*. *Azadinium caudatum* var. *margalefii* strains 9-E13 and AC1 (from Scotland) shared identical sequences. *Azadinium* cf. *zhuanum* strain 32-R1 and *Az. zhuanum* strain TIO205 (from China) shared 97.1% similarity.

For ITS-5.8S rRNA gene sequences comparison, all three strains of *Az. galwayense* shared identical sequences. All six strains of *Az. perfusorium* selected for ITS sequencing shared identical sequences, too. *Azadinium caudatum* var. *margalefii*

strains 9-E13 and AC1 (from Scotland) shared 99.7% similarity. *Azadinium* cf. *zhuanum* strain 32-R1 and *Az. zhuanum* strain TIO205 (from China) shared 89.6% similarity. Uncorrected pairwise genetic distances among some selected *Azadinium* and *Amphidoma* strains and species based on ITS-5.8S rRNA gene sequences ranged from 0.05 to 0.30 (Table 3).

The maximum likelihood (ML) and Bayesian inference (BI) analysis based on concatenated SSU, ITS-5.8S and partial LSU rRNA gene sequences yielded similar phylogenetic trees. The BI tree was illustrated in Fig. 15. The family Amphidomataceae was well resolved with strong support (0.95 BPP/94 BS) consisting of two clades. The first clade comprising *Amphidoma* and two *Azadinium* species (*Az. concinnum* Tillmann & Nézan and *Az. perforatum* Tillmann, Wietkamp & H.Gu) was not supported, and the second clade comprising all other *Azadinium* species was well supported (0.99 BPP/99 BS). The new species *Az. galwayense* was monophyletic with maximal support (1.00 BPP/100 BS) and diverged earliest in the second clade, followed by *Az. perfusorium* which was monophyletic too with maximal support and formed a sister clade of *Azadinium dexteroporum* Percopo & Zingone with low support (0.92 BPP/16 BS). The new *Az. caudatum* var. *margalefii* strain 9-E13 grouped together with other two strains of *Az. caudatum* var. *margalefii* with maximal support and made a sister clade of *Az. caudatum var. caudatum* (Halldal) Nézan & Chomérat with maximal support. Strain 32-R1 of *Az.* cf. *zhuanum* formed a sister clade of Pacific *Az. zhuanum* with maximal support.

The ITS2 secondary structure of *Az.* cf. *zhuanum* strain 32-R1 (North Atlantic) and *Az. zhuanum* strain TIO205 (Pacific) was predicted. Both of them showed four main helices (I, II, III, IV) and displayed at least one compensatory base change (CBC, compensatory change on both side of a helix pairing) in helices II, III and IV (Fig. S8 in the Supporting Information).

qPCR assay specificity

No amplification in the current *Az. spinosum*, *Az. poporum* and *Am. languida* qPCR assays was observed for any of the selected non-target strains of *Az. galwayense*, *Az. perfusorium*, *Az.* cf. *zhuanum* and *Az. caudatum* var. *margalefii*. In contrast, the amphidomatacean (family-specific) assay revealed positive signals for all these tested (target) strains.

DISCUSSION

The two new species - morphology

Both morphological and molecular sequencing approaches clearly show that among the newly established strains from Irish waters there are two new species of *Azadinium*. The new species *Az. galwayense* and *Az. perfusorium* conform with all features described as characteristic for the genus *Azadinium* (Tillmann *et al*. 2009). They are very similar to several other species of *Azadinium* in size and overall shape, but both of them possesses a distinctive and unique combination of features, which unambiguously differentiate them from other *Azadinium*. Previous works on *Azadinium* underline the importance of the ventral pore (vp) position as diagnostic feature for species discrimination. The amphidomatacean vp is larger than regular thecal pores, surrounded by a platelet-like structure, and has different and species-specific positions on the ventral part of the epitheca (Tillmann *et al*. 2012a; Tillmann & Akselman 2016). Both new species have the vp on the cells' right side of the pore plate and thus are distinct from *Az. spinosum*, *Az. obesum* Tillmann & Elbrächter, *Az. polongum* Tillmann, and *Az. asperum* Tillmann (vp on the left side of plate 1′), from *Az. poporum*, *Az. dalianense*, *Az. trinitatum* Tillmann & Nézan, *Az. cuneatum* Tillmann & Nézan (vp on the left side of the pore plate), and *Az. caudatum* var. *caudatum* (vp on the right side of plate 1′; see table 3 in Tillmann *et al*. 2014a). There is one species likely to be *Azadinium* where the vp position is unknown: *Gonyaulax parva* Ramsfjell described from the Norwegian Sea and Iceland (Ramsfjell 1959) corresponds to the plate tabulation of *Azadinium* (and thus should be transferred to *Azadinium* at a later stage) but differs from the newly described species by its absence of an antapical spine and because all three intercalary plates of *G. parva* are of small size (Ramsfjell 1959).

Thus we are left for a detailed comparison with species that have the vp on the cells' right side of the pore plate, which are *Az. caudatum* var. *margalefii*, *Az. concinnum*, *Az. dexteroporum*, *Az. luciferelloides* Tillmann & Akselman, *Az. zhuanum*, and *Az. perforatum* (Table 4). Of those, *Azadinium caudatum* var. *margalefii* is not listed in Table 4 because this taxon is easily recognizable even in LM as distinctly different to all new species in terms of general size and shape of the cell and of the antapical spine (compare Fig. 14 with Figs 4, 8, and 11).

Evaluating the taxonomic status of the new Atlantic strain 32-R1, which we here designated as *Az.* cf. *zhuanum*, is more difficult. In terms of cell size, shape and the presence of a solid and fairly large antapical spine, this new strain without doubt conform with the original description of *Az. zhuanum* described from China, Pacific (Luo *et al*. 2017). However, for other traits, strain 32-R1 differs from the original *Az. zhuanum* description: with a nucleus positioned in the hyposome strain 32-R1 is different to the species description of *Az. zhuanum*, where the nucleus was reported to be located in the episome. In addition, the dominant plate pattern of the type strain TIO205 was reported to consist of four apical plates and two intercalary plates, whereas the new Atlantic strain 32-R1 has a dominant plate pattern of only three apical plates and two intercalary plates. Moreover, there are significant molecular differences between the new Atlantic strain 32-R1 and the Chinese *Az. zhuanum* strains. The ITS-based genetic distance of 0.11 is for example significantly larger than the distance between the two species described here as new (i.e. 0.06, Table 3). Moreover, there are three CBCs in the ITS2 secondary structure which further indicates that the new Atlantic strain 32-R1 might be separated at the species level from the Pacific *Az. zhuanum*. However, the morphological differences mentioned above (nuclear position, number of apical plates) have to be considered very carefully, as only one strain of Atlantic *Az.* cf. *zhuanum* and Pacific *Az. zhuanum* has yet been investigated in detail. With respect to nucleus position, it is known that shape and position of the nucleus may change during cell division (see Fig. 11h this

Table 3. Uncorrected genetic p-distance between ITS-5.8S rRNA gene sequences of selected *Azadinium*/*Amphidoma* species/strains. Asterisks (*) denote strains obtained in this study

species	strain	Italy	1C6	A2D11	UTHC8	3D6	2E10	AZCH02	3D9	SHETB2	SM1	5-B8	35-R7	9-E13	TIO205	32-R1	H-1E9
Az. dexteroporum	Italy	-															
Az. concinnum	1C6	0.26	-														
Az. trinitatum	A2D11	0.15	0.25	-													
Az. poporum	UTHC8	0.15	0.27	0.07	-												
Az. cuneatum	3D6	0.15	0.26	0.09	0.08	-											
Az. obesum	2E10	0.14	0.26	0.05	0.05	0.07	-										
Az. dalianense	AZCH02	0.16	0.28	0.09	0.08	0.11	0.07	-									
Az. spinosum	3D9	0.16	0.25	0.06	0.08	0.10	0.05	0.09	-								
Az. polongum	SHETB2	0.21	0.27	0.18	0.17	0.18	0.16	0.19	0.16	-							
Am. languida	SM1	0.28	0.26	0.28	0.27	0.26	0.27	0.28	0.29	0.28	-						
Az. perfusorium	5-B8*	0.10	0.24	0.11	0.12	0.13	0.10	0.13	0.12	0.18	0.26	-					
Az. galwayense	35-R7*	0.10	0.23	0.11	0.12	0.12	0.10	0.12	0.11	0.17	0.25	0.06	-				
Az. caudatum var. *margalefii*	9-E13*	0.18	0.26	0.17	0.18	0.19	0.17	0.18	0.17	0.22	0.27	0.16	0.15	-			
Az. zhuanum	TIO205	0.20	0.28	0.16	0.18	0.18	0.16	0.18	0.17	0.22	0.27	0.16	0.16	0.21	-		
Az. cf. *zhuanum*	32-R1*	0.23	0.29	0.19	0.20	0.21	0.19	0.22	0.20	0.25	0.27	0.18	0.18	0.23	0.11	-	
Am. parvula	H-1E9	0.29	0.26	0.28	0.28	0.29	0.28	0.29	0.28	0.28	0.19	0.26	0.25	0.27	0.28	0.29	-
Az. perforatum	AZA2H	0.28	0.28	0.28	0.29	0.28	0.27	0.27	0.28	0.30	0.30	0.26	0.24	0.28	0.30	0.29	0.28

study, Tillmann & Elbrächter 2013), and thus nucleus position might not be a constant and reliable trait used for species differentiation. Likewise, the significance of the dominant apical plate number (three for *Az.* cf. *zhuanum* strain 32-R1 and four for *Az. zhuanum* type strain TIO205) is unclear at the moment because for both strains intra-clonal deviations from the dominant number of apical plates are known, and, again, only one strain of each has been investigated in detail. From the Atlantic side there are no other strains of *Az. zhuanum*/*Az.* cf. *zhuanum* currently available. However, another Chinese *Az. zhuanum* strain (TIO213, Luo *et al*. 2017) which is still available in our lab now, with new additional analyses, revealed that the nucleus position, while being dominantly located in the episome, can also be located in the center of the cell or in the hyposome (H. Gu, unpublished data). Moreover, a new evaluation of the epithecal plate pattern of that strain indicated that almost half of the cells had three or four apical plates, respectively (H. Gu, unpublished data). The limited number of available strains and the indications of large variability in both nucleus position and number of apical plates in Chinese *Az. zhuanum* prevented us from erecting a new species for the Atlantic strain 32-R1 and argue to await future studies with more strains for a final conclusion.

Both *Az. galwayense* and *Az. perfusorium* may be differentiated from each other at the LM level using the location of the pyrenoid, which consistently is anterior in *Az. galwayense* and posterior in *Az. perfusorium*. However, this trait is of little help differentiating the new species from other *Azadinium*. In fact, pyrenoid position of *Az. perfusorium* is identical to *Az. dalianense* (as is the presence of an antapical spine) (Luo *et al*. 2013; Kim *et al*. 2017; Wietkamp *et al*. 2019a) such that this new species initially on board was cursorily identified as *Az. dalianense*. Moreover, in *Az. zhuanum* and in *Az.* cf. *zhuanum* strain 32-R1 there is intra-clonal variability in pyrenoid position (Luo *et al*. 2017; this study: Fig. 11). For some *Azadinium* species in culture, the number of pyrenoids was found to be variable as well (Tillmann *et al*. 2014a; Kim *et al*. 2017), and all this variability speaks against considering pyrenoid position/number as a reliable taxonomic character.

Thus, details of thecal plates are additionally needed as diagnostic traits. Both *Az. galwayense* and *Az. perfusorium* differ from *Az. zhuanum* by the differing number in anterior intercalary plates (Luo *et al*. 2017; this study). *Azadinium dexteroporum* is smaller than *Az. galwayense* or *Az. perfusorium* and can be differentiated from both new species by its most characteristic feature, i.e. the vp, which is located at the distal end of the more or less elongated right side of an asymmetric pore plate (Percopo *et al*. 2013; Tillmann *et al*. 2015, 2020). The recently described *Az. perforatum* (Tillmann *et al*. 2020) is slightly larger and slender compared to *Az. galwayense* and *Az. perfusorium*, lacks a pyrenoid with starch sheath, and has a very tiny spine. Moreover, this species is unique by the presence of thecal pores on the pore plate (Tillmann *et al*. 2020). Different to the new species, *Az. concinnum* lacks a pyrenoid with starch sheath, and this species has very small lateral, dorsal apical plates and intercalary plates and thus all symmetrically arranged precingular plates are very high (Tillmann *et al*. 2014a). A differentiation of both *Az. galwayense* and *Az. perfusorium* from *Az. luciferelloides* has to be based on SEM observations only, as for this species no live material and/or LM pictures are available (Tillmann &

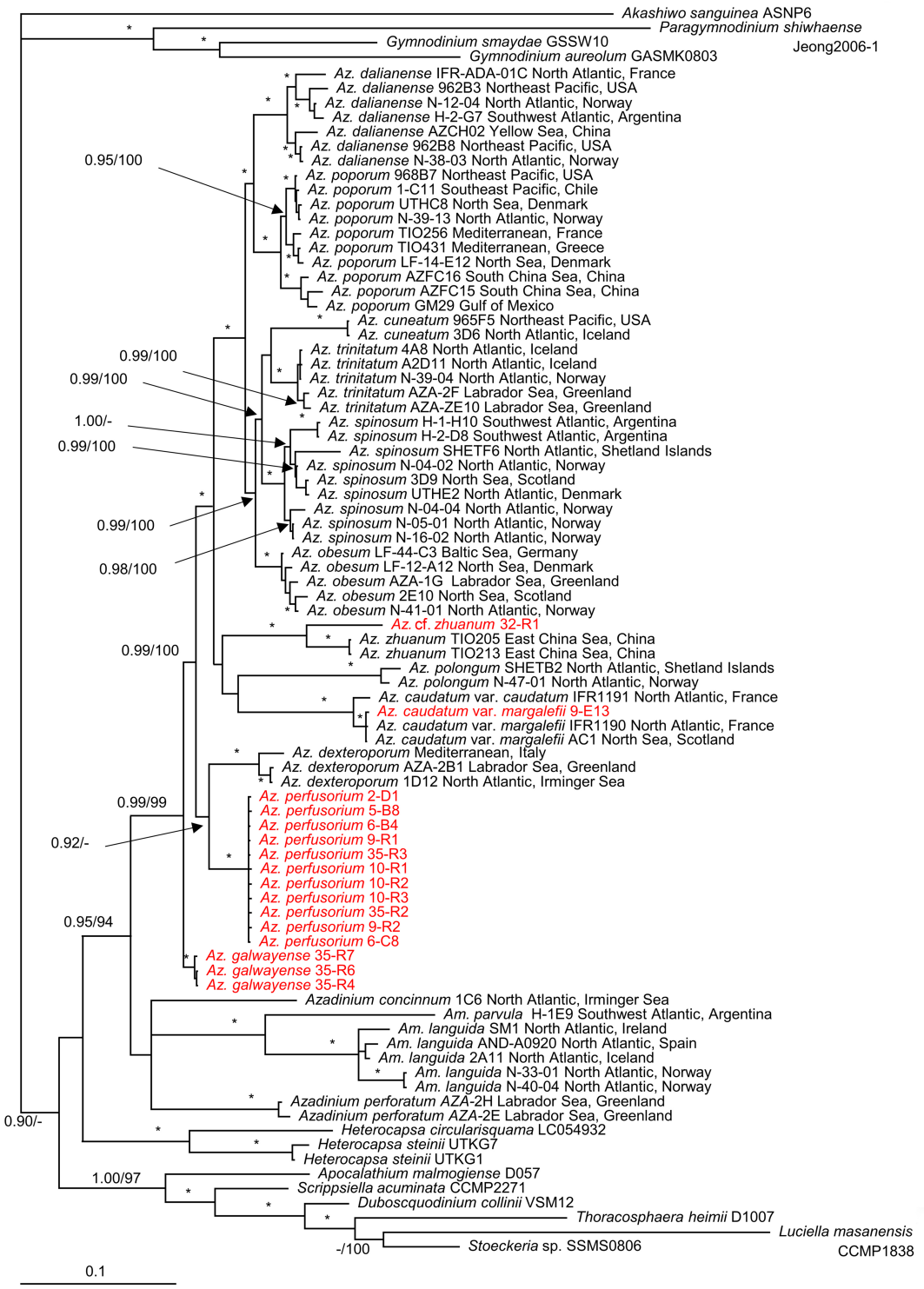

Fig 15. Molecular phylogeny of *Azadinium* and *Amphidoma* inferred from concatenated SSU, ITS-5.8S and partial LSU rRNA gene sequences using Bayesian inference (BI). New sequences of *Azadinium perfusorium*, *Az. galwayense*, *Az. caudatum* var. *margalefii* and *Az.* cf. *zhuanum* are indicated in red. Scale bar indicates number of nucleotide substitutions per site. Numbers on branches are statistical support values (left, Bayesian posterior probabilities, BPP; right, ML bootstrap support values, BS). Bootstrap values >50% and posterior probabilities above 0.9 are shown. Asterisks (*) indicate maximal support (pp = 1.00 in BI and bootstrap = 100% in ML, respectively). [Color figure can be viewed at wileyonlinelibrary.com]

Table 4. Compilation of morphological features of *Azadinium* species (including the two new species and *Az.* cf. *zhuanum*) with a ventral pore located on the cells right side of the pore plate

	Az. zhuanum	*Az.* cf. *zhuanum*	*Az. dexteroporum*	*Az. perforatum*	*Az. concinnum*	*Az. luciferelloides*	*Az galwayense*	*Az perfusorium*
Length range (mean)	16.8–21.6 (18.5)	14.9–20.1 (17.2)	7.0–10.0 (8.5)	15.3–20.0 (18.0)	8.0–11.5 (9.5)	9.4–14.1 † (11.1)	11.4–18.4 (13.7)	11.3–18.0 (14.2)
Width range (mean)	12.5–18.8 (14.8)	12.3–17.5 (14.2)	5.0–8.0 (6.2)	9.9–14.4 (12.6)	5.6–8.3 (6.6)	6.6–10.1 † (7.9)	8.3–15.1 (10.6)	8.3–13.5 (10.7)
L/W ratio	1.3	1.2	1.4	1.5	1.4	1.4	1.3	1.3
Nucleus	Round anterior	Round posterior	Round posterior	Ellipsoid median	Round posterior	Unknown	Round/oval posterior	Round/oval median
Antapical projection	Spine	Spine	Spine	Tiny spine	Spine	Spine	Spine	Spine
Stalked pyrenoid	1, epi- OR hyposome	1, epi- OR hyposome	1, episome	None	None	Unknown	1, episome	1, hyposome
1″ in contact 1a	Yes	Yes	Yes	No	No	Yes	No	Yes
Dominant nr. apicals and intercalaries	4, 2	3, 2	4, 3	4, 3	4, 3	4, 3	4, 3	4, 3
Ventral pore position	Pore plate, right side	Pore plate, right side	End of pore plate, right side	Pore plate, right side, notch in po	Pore plate, right side, notch in po	Pore plate, right side, notch in po	Pore plate, right side	Pore plate, right side, notch in po
Pore plate symmetry	Suture to 1′ almost symmetric	Suture to 1′ almost symmetric	Suture to 1′ strongly asymmetric	Suture to 1′ almost symmetric	Suture to 1′ almost symmetric	Suture to 1′ almost symmetric	Suture to 1′ almost symmetric	Suture to 1′ almost symmetric
Thecal pores on the pore plate	No	No	No	Yes	No	No	No	No
Relative size 1a/3a	Large	Large	Small	Small	Very small	Small	Small	Large
Configuration 2a	No plate 2a	No plate 2a	Quadra (penta) §	Penta	Penta	Quadra (penta) ††	Penta	Quadra
Relative size apical plates	Medium	Medium	Small	Medium	Small	Small	Medium	Medium
Size and arrangement of precingular plates	Plate 3″ mid-dorsal	Plate 3″ mid-dorsal	Plate 3″ mid-dorsal	Large, symmetrically arranged, plate 3″ and 4″ mid-dorsal	Large, symmetrically arranged, plate 3″ and 4″ mid-dorsal	Plate 3″ mid-dorsal	Both plates 3″ and 4″ mid-dorsal	Plate 3″ mid-dorsal
Records	East China Sea Yellow Sea	North Atlantic	Mediterranean, North and South Atlantic	Labrador Sea	North Atlantic	South Atlantic	North Atlantic	North Atlantic
Reference §§	a	This study	b, c	d	e	f	This study	This study

†Based on SEM only.

§Both configurations observed. The *Az. dexteroporum* strain from the Mediterranean had a quadra 2a, but in a strain from the Labrador Sea both quadra and penta 2a were documented (Tillmann *et al.* 2020).

††Based on a field population. Quadra was the dominant configuration, but pentagonal 2a plates were also recorded (Tillmann & Akselman 2016).

§§a, Luo *et al.* (2017); b, Tillmann *et al.* (2014b); c, Percopo *et al.* (2013); d, Tillmann *et al.* (2020); e, Tillmann *et al.* (2014a); f, Tillmann and Akselman (2016).

Akselman 2016) to evaluate the presence/absence of a pyrenoid and supporting confirmation based on sequence data is currently not possible. These three species may have rather subtle differences, such as the presence (*Az. galwayense* and *Az. luciferelloides*) or absence (*Az. perfusorium*) of thecal pores closely around the base of the antapical spine, whether the vp is partly located in a notch of the pore plate (*Az. luciferelloides* and *Az. perfusorium*) or not (*Az. galwayense*) or whether the plate Sa is distinctly invading the epitheca (*Az. luciferelloides* and *Az. perfusorium*) or to a much lesser degree (*Az. galwayense*). However, in SEM there are also distinct differences in epithecal plate size and arrangement among these three species (Fig. 16). These differences refer to (i) the arrangement of the medium intercalary plate 2a (pentagonal, i.e. penta-configuration; or tetragonal, i.e. quadra-configuration) and (ii) whether there is contact between plates 1″ and 1a or not. *Azadinium galwayense* differs from *Az. luciferelloides* and *Az. perfusorium* by its invariable penta-configuration of plate 2a and, related to that, by the dorsal position of both precingular plates 3″ and 4″ (Fig. 16a, b). For *Az. luciferelloides* plate 2a usually has a quadra-configuration and is in contact to plate 3″ of the precingular plates only (Fig. 16c, d), although among field specimen rarely an asymmetrical penta- configuration of plate 2a was observed (Tillmann & Akselman 2016). Moreover, *Az. galwayense* is unique among *Az. galwayense/luciferelloides/perfusorium* by a lack of contact between plate 1″ and 1a (Fig. 16a) which is present for both *Az. luciferelloides* and *Az. perfusorium* (Fig. 16c, e). Such a lack of contact between these two plates in *Azadinium* is otherwise present in *Az. obesum* and *Az. cuneatum* (Tillmann *et al*. 2010, 2014a). A lack of contact between plate 1a and 1″ was also noted in a field population of *Az. polongum* from Peru (Tillmann *et al*. 2017a), whereas such a contact is consistently present in the type material of *Az. polongum* (Tillmann *et al*. 2012b). However, with a lack of sequence data for the Peru field population its conspecificity with *Az. polongum* is unclear at present. The outstanding and most important difference between *Az. perfusorium* and *Az. luciferelloides* is the size of the lateral anterior intercalary plates 1a and 3a, which are distinctly and consistently larger in *Az. perfusorium* (Fig. 16e, f) compared to the small size in *Az. luciferelloides* (Fig. 16c, d). We consider this stable trait as sufficient morphological evidence to differentiate *Az. perfusorium* from *Az. luciferelloides*, but further attempts to obtain sequence data of *Az. luciferelloides* are needed for verification.

Molecular phylogeny

The morphological diagnosis of *Az. galwayense* and *Az. perfusorium* as new species is clearly supported by the molecular phylogenetic analysis, as strains from these species are placed in well-defined separate clusters in the phylogenetic tree (Fig. 15). The new Atlantic strain designated as *Az.* cf. *zhuanum* forms a sister clade with Pacific strains of *Az. zhuanum* with maximal support. The genetic distance between Atlantic and Pacific strains based on ITS-5.8S rRNA gene sequences reaches 0.11, compared to 0.06 between *Az. galwayense* and *Az. perfusorium*. Moreover, at least three CBCs in ITS2 (Fig. S8 in the Supporting Information) were revealed between *Az.* cf. *zhuanum* and *Az. zhuanum*. This may indicate that they belong to different species, as single CBC in helix III have been suggested to indicate gamete incompatibility and therefore separate species (Coleman 2009). But – as discussed above – for a final conclusion on the taxonomic status of strain 32-R1, detailed morphological analysis of additional strains is needed.

Generally, adding the new sequences in the phylogenetic analysis fosters previous notions of the monophyly of Amphidomataceae. However, as noted previously (Tillmann *et al*. 2018b, 2020), both *Az. concinnum* and *Az. perforatum* are placed in a clade with *Am. languida* and *Am. parvula*, but with only low statistical support (0.55 BPP/45 BS). In the *Azadinium* clade, *Az. galwayense* is the earliest diverging species followed by a clade where *Az. perfusorium* and *Az. dexteroporum* are sister groups. Species of these early diverging Amphidomataceae groups, i.e. *Am. languida*, *Az. concinnum*, *Az. perforatum*, *Az. galwayense*, *Az. perfusorium* and *Az. dexteroporum*, share a right-side apical position of the ventral pore indicating that this is an ancestral trait in the Amphidomataceae. Morphological agreements of *Az. galwayense* with *Az. concinnum* and *Az. perforatum* with respect to a symmetrically arranged pentagonal plate 2a above the two symmetrical dorsal precingular plates 3″ and 4″ (Table 4) are not reflected in the current molecular tree. Generally, the currently unresolved position of e.g. *Az. concinnum* in phylogenetic trees being either within the genus *Azadinium* (Tillmann *et al*. 2020) or outside *Azadinium* and more close to *Amphidoma* (this study), the limited number of strains available for *Az. concinnum* and *Az. perforatum*, and the current lack of sequence data especially for additional species of *Amphidoma* prevent from a final conclusion about the generic level differentiation within Amphidomataceae.

Diversity of Amphidomataceae in Irish waters

The present description of two new species of *Azadinium* and the first record of *Az.* cf. *zhuanum* from Irish coastal waters add significantly to the knowledge on the diversity of Amphidomataceae in the area. Known for many years in Ireland is the large and easy to identify species *Az. caudatum* with both varieties (var. *margalefii* and var. *caudatum*) (Dodge 1981; O'Boyle & Raine 2007), which is regularly recorded in the Irish plankton monitoring program. The new strain of *Az. caudatum* var. *margalefii* now, based on LC–MS/MS analysis, importantly indicate that Irish populations of the taxon are non-toxigenic confirming previous analyses of a Scottish strain (Tillmann *et al*. 2014b).

All strains of the two new species lack any AZA, which foster the notion that AZA production for Amphidomataceae (now known for only four of the 16 species tested so far) is more the exception than the rule. However, strain variability on AZA production potential is known for *Az. dexteroporum*, where a Mediterranean strain is a producer of various AZA (Rossi *et al*. 2017) whereas two strains from the North Atlantic with slightly different sequence data compared to the Mediterranean *Az. dexteroporum* strain are not (Tillmann *et al*. 2015, 2020). It thus may be premature to claim non-toxigenicity for the new species, but at least for *Az. perfusorium* with multiple strains from multiple stations it is quite likely that non-toxigenicity of Irish populations of this species is a stable trait. No AZA was detected in *Az.* cf. *zhuanum* 32-R1 or in

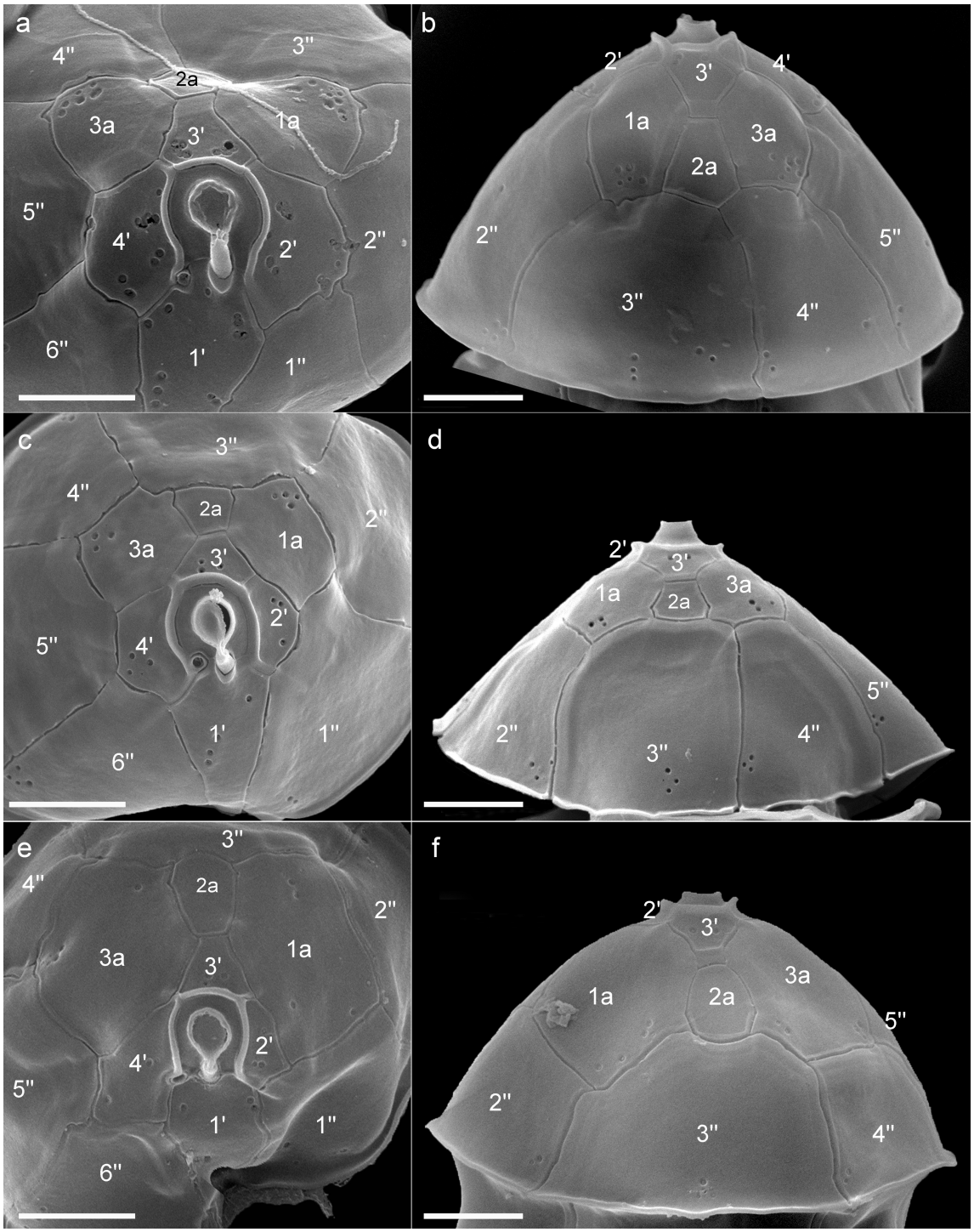

Fig 16. Comparison of epithecal plates of (a, b) *Az. galwayense* (strain 35-R7), (c, d) *Az. luciferelloides* (from a field sample), and (e, f) *Az. perfusorium* (strain 5-B8). Scale bars: 2 μm. Figure 16 c and d are adapted from Tillmann and Akselman (2016).

Az. caudatum var. *margalefii* 9-E13, supporting non-toxigenicity of these taxa reported previously (Tillmann *et al*. 2014b; Luo *et al*. 2017).

The diversity of Amphidomataceae in Irish waters also includes toxigenic species. Both *Az. spinosum* and *Am. languida* are known to be present in the area based on studies on a single strain each (Salas *et al*. 2011; Tillmann *et al*. 2012a) isolated from Bantry Bay in Southern Ireland. In addition, both species are repeatedly recorded using specific qPCR assays of field surveys (Wietkamp *et al*. 2019b, 2020) and/or the Irish monitoring program (Clarke 2020; Clarke *et al*. 2020). The third AZA producing species of Irish waters, *Az. poporum*, has been recorded from the area based on positive qPCR signals before (Wietkamp *et al*. 2020), but local strains

are not yet available for confirmation. Another non-toxigenic species, *Az. obesum*, also can be added to the Irish list of species, as this species is occasionally detected by its specific PCR probe (Clarke *et al*. 2020) and for which we have unpublished SEM confirmation (R. Salas unpublished) from a western Ireland plankton sample. LM micrographs obtained on-board of the AZAHAB cruise indicate at least one more yet undescribed amphidomatacean species (*Azadinium* sp. 1) characterized by a fairly asymmetric shape of the epitheca (Fig. 2h). In conclusion, the diversity of Amphidomataceae in Irish waters is high and comprise the presence of at least nine different species (*Az. spinosum*, *Az. poporum*, *Am languida*, *Az. caudatum*, *Az. obesum*, *Az.* cf. *zhuanum*, *Az. galwayense* sp. nov., *Az. perfusorium* sp. nov., and *Azadinium* sp. 1). A high diversity of Amphidomataceae has been reported before from various areas including North Pacific coastal waters (Kim *et al*. 2017), North Atlantic Subarctic waters (Tillmann *et al*. 2020), the Norwegian coast (Tillmann *et al*. 2018a) or the Argentinean shelf (Tillmann & Akselman 2016; Tillmann 2018; Tillmann *et al*. 2019), and thus seem to be the rule and not an exception.

Abundance of non-toxigenic species in the Irish coastal area are poorly known (except that it is known that *Az. caudatum* is regularly present but never in high abundances). The high number of strains of *Az. perfusorium* obtained from five different stations indicate that non-AZA producers are widespread and potentially abundant as well. This, of course complicates any LM based early warning plankton monitoring program aiming at detecting alarming levels of toxigenic Amphidomataceae, as small non-toxigenic species including *Az. galwayense, Az.* cf. *zhuanum* and *Az. perfusorium* can hardly be distinguished by routine LM from toxigenic *Azadinium spinosum*. The presence of other yet undetermined AZA producing species in the area can of course not be ruled out, but the lack of new toxigenic species among the multiple new isolates of the survey provide evidence that monitoring the previously known Atlantic AZA producers (*Az. spinosum*, *Az. poporum* and *Am. languida*) using existing specific molecular detection methods is adequate from an AZA early warning perspective. Testing DNA of all new strains with all three specific qPCR assays (*Az. spinosum*, *Az. poporum* and *Am. languida*) also excludes false-positive cross reactivity of the two new non-toxigenic species and of *Az.* cf. *zhuanum* and *Az. caudatum* var. *margalefii* with the AZA-producer detection assays.

ACKNOWLEDGMENTS

The authors thank Caroline Cusack, Paula Hynes and Joe Silke (Marine Institute, Galway, Ireland), as well as Luisa Hintze and Karina Krapf (AWI, Bremerhaven, Germany) for on-board technical support. Thomas Max and Anne Müller (both AWI Bremerhaven, Germany) are thanked for continued support in laboratory work and AZA analysis. This work was supported by funding of the German Ministry for Education and Research (project RIPAZA, 03F0763A) and by the PACES II research program of the Alfred-Wegener-Institute as part of the Helmholtz Foundation initiative in Earth and Environment.

Open access funding enabled and organized by Projekt DEAL. [Correction added on 06 March 2021, after first online publication: Open Access funding information was added to the 'Acknowledgments' section.]

REFERENCES

Adachi, M., Sako, Y. and Ishida, Y. 1996. Analysis of *Alexandrium* (Dinophyceae) species using sequences of the 5.8S ribosomal DNA and internal transcribed spacer regions. *J. Phycol.* **32**: 424–32.

Álvarez, G., Uribe, E., Ávalos, P., Mariño, C. and Blanco, J. 2010. First identification of azaspiracid and spirolides in *Mesodesma donacium* and *Mulinia edulis* from northern Chile. *Toxicon* **55**: 638–41.

Amzil, Z., Sibat, M., Royer, F. and Savar, V. 2008. First report on azaspiracid and yessotoxin groups detection in French shellfish. *Toxicon* **52**: 39–48.

Anonymous 2004. Regulation (EC) No 853/2004 of the European Parliament and of the Council of 29 April 2004 laying down specific hygiene rules for on the hygiene of foodstuffs. *J. Eur. Union* **30**: 1–151.

Braña Magdalena, A., Lehane, M., Krys, S., Fernández, M. L., Furey, A. and James, K. J. 2003. The first identification of azaspiracids in shellfish from France and Spain. *Toxicon* **42**: 105–8.

Boc, A., Diallo, A. B. and Makarenkov, V. 2012. T-REX: a web server for inferring, validating and visualizing phylogenetic trees and networks. *Nucleic Acids Res.* **40**: 573–9.

Clarke, D. 2020. New insights and perspectives from 20 years of monitoring algal events in Irish coastal waters. *In* Clarke, D. and Gilmartin, M. (Eds). *Proceedings of the 11th Irish Shellfish Safety Workshop, Marine Environment and Health Series No. 41*. Marine Institute, Galway. In press.

Clarke, D., Salas, R., Hynes, P., McCarthy, A., Walsh, D. and Silke, J. 2020. PCR assays for the detection of ASP, DSP, PSP and AZP toxigenic producing phytoplanktonic species in Irish coastal waters. *In* Hess, P. (Ed.). *Proceedings of the 18th Conference on Harmful Algae Blooms*. ISSHA, Nantes, pp. 19–24.

Coleman, A. W. 2009. Is there a molecular key to the level of "biological species" in eukaryotes? A DNA guide. *Mol. Phylogenet. Evol.* **50**: 197–203.

Dodge, J. D. 1981. *Provisional Atlas of the Marine Dinoflagellates of the British Isles*. Biological Records Centre, Huntingdon.

Hall, T. 1999. BioEdit: a user-friendly biological sequence alignment editor and analysis program for Windows 95/98/NT. *Nucleic Acids Symp. Ser.* **41**: 95–8.

James, K. J., Lehane, M., Ramstad, H. *et al*. 2002. First evidence of an extensive northern European distribution of azaspiracid poisoning (AZP) toxins in shellfish. *Toxicon* **40**: 909–15.

Katoh, K. and Standley, D. M. 2013. MAFFT multiple sequence alignment software version 7: improvements in performance and usability. *Mol. Biol. Evol.* **30**: 772–80.

Keller, M. D., Selvin, R. C., Claus, W. and Guillard, R. R. L. 1987. Media for the culture of oceanic ultraphytoplankton. *J. Phycol.* **23**: 633–8.

Kim, J. H., Tillmann, U., Adams, N. *et al*. 2017. Identification of *Azadinium* species and a new azaspiracid from *Azadinium poporum* in Puget Sound, Washington state, USA. *Harmful Algae* **68**: 152–67.

Krock, B., Tillmann, U., John, U. and Cembella, A. D. 2009. Characterization of azaspiracids in plankton size-fractions and isolation of an azaspiracid-producing dinoflagellate from the North Sea. *Harmful Algae* **8**: 254–63.

Krock, B., Tillmann, U., Alpermann, T. J., Voß, D., Zielinski, O. and Cembella, A. D. 2013. Phycotoxin composition and distribution in plankton fractions from the German Bight and western Danish coast. *J. Plankton Res.* **35**: 1093–108.

Krock, B., Tillmann, U., Tebben, J., Trefaults, N. and Gu, H. 2019. Two novel azaspiracids from *Azadinium poporum*, and a comprehensive compilation of azaspiracids produced by Amphidomataceae (Dinophyceae). *Harmful Algae* **82**: 1–8.

López-Rivera, A., O'Callaghan, K., Moriarty, M. *et al*. 2010. First evidence of azaspiracids (AZAs): a family of lipophilic polyether

marine toxins in scallops (*Argopecten purpuratus*) and mussels (*Mytilus chilensis*) collected in two regions of Chile. *Toxicon* **55**: 692–701.

Luo, Z., Gu, H., Krock, B. and Tillmann, U. 2013. *Azadinium dalianense*, a new dinoflagellate from the Yellow Sea, China. *Phycologia* **52**: 625–36.

Luo, Z., Krock, B., Mertens, K. N. *et al*. 2017. Adding new pieces to the *Azadinium* (Dinophyceae) diversity and biogeography puzzle: non-toxigenic *Azadinium zhuanum* sp. nov. from China, toxigenic *A. poporum* from the Mediterranean, and a non-toxigenic *A. dalianense* from the French Atlantic. *Harmful Algae* **66**: 65–78.

McMahon, T. and Silke, J. 1996. West coast of Ireland; winter toxicity of unknown aetiology in mussels. *Harmful Algae News* **14**: 2.

Medlin, L. K., Elwood, H. J., Stickel, S. and Sogin, M. L. 1988. The characterization of enzymatically amplified eukaryotic 16S-like rRNA-coding regions. *Gene* **71**: 491–9.

Nézan, E., Tillmann, U., Bilien, G. *et al*. 2012. Taxonomic revision of the dinoflagellate *Amphidoma caudata*: transfer to the genus *Azadinium* (Dinophyceae) and proposal of two varieties, based on morphological and molecular phylogenetic analyses. *J. Phycol.* **48**: 925–39.

Ofuji, K., Satake, M., McMahon T. *et al*. 1999. Two analogs of azaspiracid isolated from mussels, *Mytilus edulis*, involved in human intoxication in Ireland. *Nat. Toxins* **7**: 99–102.

O'Boyle, S. and Raine, R. 2007. The influence of local and regional oceanographic processes on phytoplankton distribution in continental shelf waters off northwestern Ireland. *Biol. Environ.* **107B**: 95–109.

Percopo, I., Siano, R., Rossi, R., Soprano, V., Sarno, D. and Zingone, A. 2013. A new potentially toxic *Azadinium* species (Dinophyceae) from the Mediterranean Sea, *A. dexteroporum* sp. nov. *J. Phycol.* **49**: 950–66.

Posada, D. 2008. ModelTest: phylogenetic model averaging. *Mol. Biol. Evol.* **25**: 1253–6.

Rambaut, A., Drummond, A. J., Xie, D., Baele, G. and Suchard, M. A. 2018. Posterior summarisation in Bayesian phylogenetics using Tracer 1.7. *Syst. Biol.* **67**: 901–4.

Ramsfjell, E. 1959. Two new phytoplankton species from the Norwegian Sea, the diatom *Coscinosira poroseriata*, and the dinoflagellate *Gonyaulax parva*. *Nytt Mag. Bot.* **7**: 175–7.

Ronquist, F. and Huelsenbeck, J. P. 2003. MrBayes 3: Bayesian phylogenetic inference under mixed models. *Bioinformatics* **19**: 1572–4.

Rossi, R., Dell'Aversano, C., Krock, B. *et al*. 2017. Mediterranean *Azadinium dexteroporum* (Dinophyceae) produces AZA-35 and six novel azaspiracids: a structural study by a multi-platform mass spectrometry approach. *Anal. Bioanal. Chem.* **409**: 1121–34.

Salas, R., Tillmann, U., John, U. *et al*. 2011. The role of *Azadinium spinosum* (Dinophyceae) in the production of azaspiracid shellfish poisoning in mussels. *Harmful Algae* **10**: 774–83.

Salas, R., Tillmann, U. and Kavanagh, S. 2014. Morphology and molecular characterization of the small armoured dinoflagellate *Heterocapsa minima* (Peridiniales, Dinophyceae). *Eur. J. Phycol.* **49**: 413–28.

Satake, M., Ofuji, K., Naoki, H. *et al*. 1998. Azaspiracid, a new marine toxin having unique spiro ring assemblies, isolated from Irish mussels, *Mytilus edulis*. *J. Am. Chem. Soc.* **120**: 9967–8.

Scholin, C. A., Herzog, M., Sogin, M. and Anderson, D. M. 1994. Identification of group- and strain-specific genetic markers for globally distributed *Alexandrium* (Dinophyceae). II. Sequence analysis of a fragment of the LSU rRNA gene. *J. Phycol.* **30**: 999–1011.

Smith, K. F., Rhodes, L., Harwood, D. T. *et al*. 2016. Detection of *Azadinium poporum* in New Zealand: the use of molecular tools to assist with species isolations. *J. Appl. Phycol.* **28**: 1125–32.

Stamatakis, A. 2006. RAxML-VI-HPC: maximum likelihood-based phylogenetic analyses with thousands of taxa and mixed models. *Bioinformatics* **22**: 2688–90.

Swofford, D. L. 2002. *PAUP*: Phylogenetic Analysis Using Parsimony (* and Other Methods), Version 4.0b10*. Sinauer Associates, Sunderland, MA.

Taleb, H., Vale, P., Amanhir, R., Benhadouch, A., Sagou, R. and Chafik, A. 2006. First detection of azaspiracids in mussels in north West Africa. *J. Shellfish. Res.* **25**: 1067–70.

Tillmann, U., Elbrächter, M., Krock, B., John, U. and Cembella, A. 2009. *Azadinium spinosum* gen. et sp. nov. (Dinophyceae) identified as a primary producer of azaspiracid toxins. *Eur. J. Phycol.* **44**: 63–79.

Tillmann, U., Elbrächter, M., John, U., Krock, B. and Cembella, A. 2010. *Azadinium obesum* (Dinophyceae), a new nontoxic species in the genus that can produce azaspiracid toxins. *Phycologia* **49**: 169–82.

Tillmann, U., Elbrächter, M., John, U. and Krock, B. 2011. A new non-toxic species in the dinoflagellate genus *Azadinium*: *A. poporum* sp. nov. *Eur. J. Phycol.* **46**: 74–87.

Tillmann, U., Salas, R., Gottschling, M., Krock, B., O'Driscoll, D. and Elbrächter, M. 2012a. *Amphidoma languida* sp. nov. (Dinophyceae) reveals a close relationship between *Amphidoma* and *Azadinium*. *Protist* **163**: 701–19.

Tillmann, U., Soehner, S., Nézan, E. and Krock, B. 2012b. First record of *Azadinium* from the Shetland Islands including the description of *A. polongum* sp. nov. *Harmful Algae* **20**: 142–55.

Tillmann, U. and Elbrächter, M. 2013. Cell division in *Azadinium spinosum* (Dinophyceae). *Bot. Mar.* **56**: 399–408.

Tillmann, U., Gottschling, M., Nézan, E., Krock, B. and Bilien, G. 2014a. Morphological and molecular characterization of three new *Azadinium* species (Amphidomataceae, Dinophyceae) from the Irminger Sea. *Protist* **165**: 417–44.

Tillmann, U., Krock, B. and Taylor, B. 2014b. *Azadinium caudatum* var. *margalefii*, a poorly known member of the toxigenic genus *Azadinium* (Dinophyceae). *Mar. Biol. Res.* **10**: 941–56.

Tillmann, U., Salas, R., Jauffrais, T., Hess, P. and Silke, J. 2014c. AZA: the producing organisms - biology and trophic transfer. *In* Botana, L. M. (Ed.). *Seafood and Freshwater Toxins*. CRC Press, Boca Raton, FL, pp. 773–98.

Tillmann, U., Gottschling, M., Nézan, E. and Krock, B. 2015. First record of *Azadinium dexteroporum* and *Amphidoma languida* (Amphidomataceae, Dinophyceae) from the Irminger Sea off Iceland. *Mar. Biodiv. Rec.* **8**: 1–11.

Tillmann, U. and Akselman, R. 2016. Revisiting the 1991 algal bloom in shelf waters off Argentina: *Azadinium luciferelloides* sp. nov. (Amphidomataceae, Dinophyceae) as the causative species in a diverse community of other amphidomataceans. *Phycol. Res.* **64**: 160–75.

Tillmann, U., Borel, C. M., Barrera, F. *et al*. 2016. *Azadinium poporum* from the argentine continental shelf, southwestern Atlantic, produces azaspiracid-2 and azaspiracid-2 phosphate. *Harmful Algae* **51**: 40–55.

Tillmann, U., Sánchez-Ramírez, S., Krock, B. and Bernales-Jiménez, A. 2017a. A bloom of *Azadinium polongum* in coastal waters off Peru. *Rev. Biol. Mar. Oceanog.* **52**: 591–610.

Tillmann, U., Trefault, N., Krock, B., Parada-Pozo, G., De la Iglesia, R. and Vásquez, M. 2017b. Identification of *Azadinium poporum* (Dinophyceae) in the Southeast Pacific: morphology, molecular phylogeny, and azaspiracid profile characterization. *J. Plankton Res.* **39**: 350–67.

Tillmann, U. 2018. Electron microscopy of a 1991 spring plankton sample from the Argentinean shelf reveals the presence of four new species of Amphidomataceae (Dinophyceae). *Phycol. Res.* **66**: 269–90.

Tillmann, U., Edvardsen, B., Krock, B., Smith, K. F., Paterson, R. F. and Voß, D. 2018a. Diversity, distribution, and azaspiracids of

Amphidomataceae (Dinophyceae) along the Norwegian coast. *Harmful Algae* **80**: 15–34.
Tillmann, U., Gottschling, M., Guinder, V. and Krock, B. 2018b. *Amphidoma parvula* (Amphidomataceae), a new planktonic dinophyte from the argentine sea. *Eur. J. Phycol.* **53**: 14–28.
Tillmann, U., Gottschling, M., Krock, B., Smith, K. F. and Guinder, V. 2019. High abundance of Amphidomataceae (Dinophyceae) during the 2015 spring bloom of the Argentinean shelf and a new, non-toxigenic ribotype of *Azadinium spinosum*. *Harmful Algae* **84**: 244–60.
Tillmann, U., Wietkamp, S., Krock, B., Tillmann, A., Voß, D. and Gu, H. 2020. Amphidomataceae (Dinophyceae) in the western Greenland area, including the description of *Azadinium perforatum* sp. nov. *Phycologia* **59**: 63–88.
Toebe, K., Joshi, A. R., Messtorff, P., Tillmann, U., Cembella, A. and John, U. 2013. Molecular discrimination of taxa within the dinoflagellate genus *Azadinium*, the source of azaspiracid toxins. *J. Plankton Res.* **35**: 225–30.
Torgersen, T., Bruun Bremmens, N., Rundberget, T. and Aune, T. 2008. Structural confirmation and occurrence of azaspiracids in Scandinavian brown crabs (*Cancer pagarus*). *Toxicon* **51**: 93–101.
Trainer, V. L., Moore, L., Bill, B. D. *et al.* 2013. Diarrhetic shellfish toxins and other lipophilic toxins of human health concern in Washington state. *Mar. Drugs* **11**: 1815–35.
Turner, A. D. and Goya, A. B. 2015. Occurrence and profiles of lipophilic toxins in shellfish harvested from Argentina. *Toxicon* **102**: 32–42.
Ueoka, R., Ito, A., Izumikawa, M. *et al.* 2009. Isolation of azaspiracid-2 from a marine sponge *Echinoclathria* sp. as a potent cytotoxin. *Toxicon* **53**: 680–4.
Vale, P., Biré, R. and Hess, P. 2008. Confirmation by LC–MS/MS of azaspiracids in shellfish from the Portuguese north-west coast. *Toxicon* **51**: 1449–56.
White, T. J., Bruns, T., Lee, S. and Taylor, J. 1990. Amplification and direct sequencing of fungal ribosomal RNA genes for phylogenetics. *In* Innis, M. A., Gelfand, D. H., Sninsky, J. J. and White, T. J. (Eds). *PCR Protocols: A Guide to Methods and Applications*. Academic Press, San Diego, CA, pp. 315–22.
Wietkamp, S., Krock, B., Gu, H., Voß, D., Klemm, K. and Tillmann, U. 2019a. Occurrence and distribution of Amphidomataceae (Dinophyceae) in Danish coastal waters of the North Sea, the Limfjord, and the Kattegat/Belt area. *Harmful Algae* **88**: 101637.
Wietkamp, S., Tillmann, U., Clarke, D. and Toebe, K. 2019b. Molecular determination and quantification of the toxigenic dinoflagellate *Amphidoma languida* (Amphidomataceae, Dinophyceae). *J. Plankton Res.* **41**: 101–13.
Wietkamp, S., Krock, B., Clarke, D. *et al.* 2020. Distribution and abundance of azaspiracid-producing dinophyte species and their toxins in North Atlantic and North Sea waters in summer 2018. *PLoS One* **15**: e0235015.
Yao, J., Tan, Z., Zhou, D., Guo, M., Xing, L. and Yang, S. 2010. Determination of azaspiracid-1 in shellfishes by liquid chromatography with tandem mass spectrometry. *Chin. J. Chromatogr.* **28**: 363–7.
Zuker, M. 2003. Mfold web server for nucleic acid folding and hybridization prediction. *Nucleic Acids Res.* **31**: 3406–15.

SUPPORTING INFORMATION

Additional Supporting Information may be found in the online version of this article at the publisher's web-site:

Fig. S1 *Az. galwayense* sp. nov. (strain 35-R7), additional micrographs.

Fig. S2 *Az. perfusorium* sp. nov. (strain 5-B8), additional SEM micrographs.

Fig. S3 *Az. perfusorium* sp. nov. (strain 5-B8), additional detailed SEM micrographs.

Fig. S4 *Az. perfusorium* sp. nov. (strain 2-D1), micrographs.

Fig. S5 *Az. perfusorium* sp. nov. (strain 2-D1), detailed SEM micrographs.

Fig. S6 *Az.* cf. *zhuanum* (strain 32-R1), epithecal plate pattern.

Fig. S7 *Az.* cf. *zhuanum* (strain 32-R1), deviating epithecal plate configurations.

Fig. S8 ITS secondary structure of *Az.* cf. *zhuanum* and *Az. zhuanum*.

Table S1 Limit of detections AZA analyses.

Table S2 Selected reaction monitoring (SRM) transitions for AZA analyses.

Table S3 GenBank accession numbers.